

The Fate of Dwarf Galaxies in Clusters and the Origin of Intracluster Stars. II. Cosmological Simulations

Hugo Martel,^{1,2} Paramita Barai,³ and William Brito²

ABSTRACT

We combine a N-body simulation algorithm with a subgrid treatment of galaxy formation, mergers, and tidal destruction, and an observed conditional luminosity function $\Phi(L|M)$, to study the origin and evolution of galactic and extragalactic light inside a cosmological volume of size $(100 \text{ Mpc})^3$, in a concordance Λ CDM model. This algorithm simulates the growth of large-scale structures and the formation of clusters, the evolution of the galaxy population in clusters, the destruction of galaxies by mergers and tides, and the evolution of the intracluster light. We find that destruction of galaxies by mergers dominates over destruction by tides by about an order of magnitude at all redshifts. However, tidal destruction is sufficient to produce intracluster light fractions f_{ICL} that are sufficiently high to match observations. Our simulation produces 18 massive clusters ($M_{\text{cl}} > 10^{14} M_{\odot}$) with values of f_{ICL} ranging from 1% to 58% at $z = 0$. There is a weak trend of f_{ICL} to increase with cluster mass. The bulk of the intracluster light ($\sim 60\%$) is provided by intermediate galaxies of total masses $10^{11} M_{\odot} - 10^{12} M_{\odot}$ and stellar masses $6 \times 10^8 M_{\odot} - 3 \times 10^{10} M_{\odot}$ that were tidally destroyed by even more massive galaxies. The contribution of low-mass galaxies to the intracluster light is small and the contribution of dwarf galaxies is negligible, even though, by numbers, most galaxies that are tidally destroyed are dwarfs. Tracking clusters back in time, we find that their values of f_{ICL} tend to increase over time, but can experience sudden changes that are sometimes non-monotonic. These changes occur during major mergers involving clusters of comparable masses but very different intracluster luminosities. Most of the tidal destruction events take place in the central regions of clusters. As a result, the intracluster light is more centrally concentrated than the galactic light. Our results support tidal destruction of intermediate-mass galaxies as a plausible scenario for the origin of the intracluster light.

Subject headings: cosmology — galaxies: clusters — galaxies: dwarfs — galaxies: interactions — methods: numerical

¹Département de physique, de génie physique et d'optique, Université Laval, Québec, QC, Canada

²Centre de Recherche en Astrophysique du Québec

³Osservatorio Astronomico di Trieste, Trieste, Italy

1. INTRODUCTION

An important contribution to the total visible light emitted by massive, X-ray galaxy clusters does not come from the galaxies themselves (Zwicky 1951; Arnaboldi 2004; Lin & Mohr 2004; Feldmeier et al. 2004a,b; West et al. 1995; Zibetti et al. 2005; Gonzalez et al. 2005; Mihos et al. 2005; Krick et al. 2006; Krick & Bernstein 2007). This so-called *intracluster light* (ICL) is attributed to intracluster stars, low surface brightness stars located outside galaxies. Intracluster stars have been directly observed (Ferguson et al. 1998; Arnaboldi et al. 2003; Gal-Yam et al. 2003; Gerhard et al. 2005). These observations reveal that the intracluster stellar population is diverse. It is mostly comprised of stars with masses of order $1M_{\odot}$, ages up to 10^{10} yr, and metallicities $[\text{Fe}/\text{H}]$ between -2 and 0 (Williams et al. 2007), but also includes red, old stars (Krick et al. 2006) AGB stars (Durrell et al. 2002), planetary nebulae (Arnaboldi et al. 1996; Feldmeier et al. 2003; Arnaboldi et al. 2004; Feldmeier et al. 2004a), novae and supernovae. (Thuan & Kormendy 1977; Crane et al. 1977; Uson 1991; Vilchez-Gomez 1994; Scheick & Kuhn 1994; Gal-Yam et al. 2003; Neill et al. 2005). The fraction of stars that contribute to the ICL increases with the mass of the clusters, and with the density of the environment: from loose groups ($< 2\%$, Castro-Rodriguez et al. 2003), to Virgo-like (10%, Feldmeier et al. 2004a; Zibetti et al. 2005) and rich clusters ($\sim 20\%$ or higher, Tyson & Fischer 1995; Feldmeier et al. 2004b; Krick & Bernstein 2007). In the cores of dense and rich clusters (like Coma) the local ICL fraction can be as high as 50% (Bernstein et al. 1995).

Several models have been suggested to explain the origin of intracluster stars. A comprehensive review of these various processes is provided by Tutukov & Fedorova (2011). Essentially, these models fall into four categories: intracluster star formation, ejection, disruption of individual galaxies, or galactic interactions.

Some models for in-situ formation of intracluster stars have been suggested. Gas-rich galaxies moving through the hot intracluster medium (ICM) might experience ram-pressure stripping. The gas extracted from the galaxies will form dense gaseous streams, which under the right conditions can fragment to form stars (Firmani & Tutukov 1992; Sun et al. 2010). This could explain the galactic tails that are observed in some galaxies such as ESO 137-001 and ESO 137-002. Hatch et al. (2008) observed a halo of diffuse UV intergalactic light surrounding a radio galaxy (the Spiderweb Galaxy), providing evidence for in-situ star formation outside galaxies. Also, tidal stripping could provide another mechanism for extracting cold gas from galaxies. In the recent simulations of Puchwein et al. (2010), up to 30% of intracluster stars formed in could gas clouds stripped from substructures infalling into the cluster center.

Supernovae explosions inside close binary systems (Blaauw 1961) can produce high-velocity stars, with velocities of several hundreds km/s. Some of these stars could have enough kinetic energy to escape the gravitational potential of the parent galaxy and reach the intracluster space (Tutukov & Fedorova 2009). However, as Tutukov & Fedorova (2011) argue, this is not an efficient mechanism for populating the intracluster space with stars. Even if ones assumes that every super-

novae produces a high-velocity star, with enough velocity to escape, the total number of intracluster stars produced by this mechanism is simply too small. Three- or four-body encounters in dense stellar systems (Poveda et al. 1967) could also produce high-velocity runaway stars, and recent simulations suggest that these stars could reach velocities as high as 400 km s^{-1} (Gvaramadze et al. 2010)

A galaxy can get disrupted if it loses some of its gravitational binding energy. A gas-rich galaxy can become unbound by losing a significant fraction of its gas. This could be caused by ram-pressure stripping, or by a galactic wind powered by SNe explosions or an AGN. Another possible mechanism is the merger of two galaxies which both host a central supermassive black hole. This will likely lead to the formation of a single galaxy with a central binary black hole. If the binding energy of this binary black hole exceeds the binding energy of the galaxy, the gravitational energy extracted from the black holes will disrupt the galaxy (Tutukov & Fedorova 2011).

While these various processes might contribute to some of the observed ICL, it is generally accepted that most intracluster stars were formed inside galaxies, and were later dispersed into the intracluster space by galaxy interactions taking place during the evolution of the clusters. This likely results from tidal stripping or tidal destruction of galaxies during close encounters (Weil et al. 1997; Gregg & West 1998; Gnedin 2003; Willman et al. 2004; Feldmeier et al. 2004a; Rudick et al. 2006; Conroy et al. 2007; Purcell et al. 2007; Barai et al. 2009, hereafter Paper I, Yang et al. 2009; Wu & Jiang 2009; Rudick et al. 2009; Puchwein et al. 2010), though an important contribution could also be provided by stars ejected during galactic mergers (Murante et al. 2007). The ICL tends to be more concentrated than the galactic light (Aguerre et al. 2005), which is interpreted as evidence for the role of galaxy collisions in the origin of the ICL (Zibetti et al. 2005). Notice that the higher rate of galaxy collisions and higher ICM pressure found in the central regions of the clusters would tend to increase the efficiency of most of the processes discussed above, the exceptions being ejection of high-velocity stars (unaffected) and SNe-driven galactic winds (possibly inhibited).

Several analytical and numerical studies of the origin and evolution of the ICL have been performed. These include studies based on analytical modeling of galaxy formation and disruption (Purcell et al. 2007), N-body simulations of large-scale structure formation combined with an analytical prescription for galaxy formation, dispersion, and merging (Napolitano et al. 2003; Rudick et al. 2006; Henriques et al. 2008; Rudick et al. 2011), and hydrodynamical simulations (Willman et al. 2004; Sommer-Larsen et al. 2005; Murante et al. 2004, 2007; Puchwein et al. 2010; Dolag et al. 2010). In these numerical studies, there is always a trade-off between having good resolution or good statistics. Napolitano et al. (2003); Willman et al. (2004); Sommer-Larsen et al. (2005), and Rudick et al. (2006) simulate either one cluster or a few clusters, so even though these clusters are simulated with high resolution, they might not be representative of the whole cluster population. At the other extreme, Murante et al. (2004, 2007) simulate a very large cosmological volume, containing a statistically significant sample of clusters, but cannot resolve the scale of dwarf galaxies. In this work, we use an algorithm which combines large-scale cosmological simulations with a semi-analytical treatment of mergers and tidal disruption. This enables us to achieve good

statistics while resolving the processes responsible for destroying dwarf galaxies.

In this paper, we focus on the relative importance of the tidal destruction and merger processes and their role in the evolution of the cluster luminosities, and do not consider the properties of the ICM. In this case, a full hydrodynamical simulation is not required, and we chose instead to combine a N-body simulation with a subgrid treatment of processes at galactic scales. We use a high-resolution N-body simulation of large-scale structure formation, as in Henriques et al. (2008) and Rudick et al. (2011), but with a different and complementary approach for galaxy formation, mergers, and tidal destruction, as described in Paper I (see § 2.1 below). Our goals are to determine (1) the fraction of galaxies of various masses destroyed by tides and mergers during the formation and evolution of the clusters, (2) the contribution of tidal destruction to the ICL, and (3) the brightness profile of the ICL resulting from tidal destruction.

2. THE NUMERICAL METHOD

2.1. N-body Simulation

Simulating the formation and destruction of dwarf galaxies in a cosmological context is quite challenging, because of the large dynamical range involved. To get statistically significant results, we need to simulate a volume of the universe large enough to contain several rich clusters. To estimate this volume, we use the cluster mass function of Bahcall & Cen (1993),

$$n_c(> M) \simeq 4 \times 10^{-5} \left(\frac{M}{M^*} \right)^{-1} e^{-M/M^*} h^3 \text{Mpc}^{-3}, \quad (1)$$

where $M^* \simeq 1.8 \times 10^{14} h^{-1} \text{M}_\odot$. Using $h = 0.704$ and $M = 10^{14} \text{M}_\odot$, we get $n_c = 2.41 \times 10^{-5} \text{Mpc}^{-3}$. For a cubic volume of size 100 Mpc, this gives 24 clusters more massive than $M = 10^{14} \text{M}_\odot$, which is probably sufficient to get good statistics. In a Λ CDM universe with $\Omega_0 = 0.268$, a $(100 \text{ Mpc})^3$ volume contains a mass of $M_{\text{tot}} = 3.69 \times 10^{16} \text{M}_\odot$. If we take the minimum mass of a dwarf galaxy to be $M_{\text{dw}} = 10^9 \text{M}_\odot$, we get $M_{\text{tot}}/M_{\text{dw}} = 3.69 \times 10^7$. Lets assume that we perform an N-body simulation with equal-mass particles, and that it takes a minimum 100 particles per galaxy to properly resolve processes such as galaxy merger and tidal destruction, we would then need 3.69 billion particles. This is comparable to some of the largest N-body simulations ever performed to this date, and would require an enormous investment in human and computer resources.

The hydrodynamical simulations of Murante et al. (2007) use three different kinds of particles (dark matter, gas, and stars) with masses $6.57 \times 10^9 \text{M}_\odot$, $9.86 \times 10^8 \text{M}_\odot$, $4.95 \times 10^8 \text{M}_\odot$, respectively. The gravity-only simulations of Rudick et al. (2011) use particles of mass $5 \times 10^8 \text{M}_\odot$, while our own simulation uses particles of mass $2.75 \times 10^8 \text{M}_\odot$. Henriques et al. (2008) used the results of the *Millenium Simulation* (Springel et al. 2005), with particles of mass $1.18 \times 10^9 \text{M}_\odot$. None of these simulations can resolve the internal structure of dwarf galaxies and properly simulate the destruction of these galaxies by mergers and tides. To solve this problem, Murante et al. (2007)

use a group finder to determine if particles belong to galaxies or are located in the intracluster space (SKID, see Stadel 2001). Rudick et al. (2011) used instead a standard “zoom-in” technique. They first performed a relatively low-resolution simulation. They selected a subset of massive clusters at redshift $z = 0$, and ran the simulation a second time, with more resolution inside the regions where these clusters formed. Puchwein et al. (2010) used the same approach, by selecting a sample of 16 clusters from the *Millenium Simulation* and resimulating them with higher resolution. This approach provides very-high resolution at reasonable computational cost. However, only a few clusters are being simulated at that high resolution. Henriques et al. (2008) use a semi-analytical model to describe galaxy formation and disruption. In this paper, we use an approach that we first introduced in Paper I. We represent each galaxy in the system (regardless of its mass) using *one single particle*. In this approach, the merger and tidal destruction of galaxies cannot be directly simulated, but instead are treated in the algorithm as subgrid physics. When two particles representing galaxies come close to each other, we can calculate the gravitational potential energy between them. We can also calculate the tidal field caused by one galaxy at the location of the other. With these, we can set rules that dictate when mergers and tidal destruction take place. This is fairly crude compared to an actual simulation of the mergers and tidal destruction events, *but is expected to make statistically correct predictions for a large number of events*. The main advantage of this approach is that it does not rely on zoom-ins, and thus enables us to simulate a larger number of clusters at high resolution. This approach was developed and tested on isolated clusters (Paper I). In this paper, we apply the same approach to a cosmological simulation, which enables us to follow the formation and evolution of a statistically significant number of clusters.

We consider a concordance Λ CDM model with $\Omega_0 = 0.268$, $\lambda_0 = 0.732$, and $h = 0.704$. We perform a high-resolution simulation in a $(100 \text{ Mpc})^3$ comoving box with periodic boundary conditions, using a Particle-Mesh (PM) algorithm with 512^3 particles and a 1024^3 mesh. The total mass in the box is $M_{\text{tot}} = 3.686 \times 10^{16} M_\odot$ and the mass per particle is $M_{\text{part}} = 2.747 \times 10^8 M_\odot$. The length resolution is 97.7 kpc comoving. We assume that dwarf galaxies of mass $M_{\text{min}} = 2 \times 10^9 M_\odot$ form inside cells where the density is 200 times the mean density. Each galaxy is represented by a “galaxy particle.” These particles are treated like PM particles, but have the ability to form, merge, and get tidally destroyed. The treatment of these processes by the algorithm is described in the following sections.

2.2. Formation of Dwarf Galaxies

To include galaxy formation in our N-body simulations, we assume that dwarf galaxies of mass $M = M_{\text{min}}$ form by monolithic collapse, while more massive galaxies form by the merger of smaller galaxies. Therefore, in our code implementation, the formation of massive galaxies by mergers is handled by the merging module, and the galaxy formation module only handles the formation of galaxies of mass $M = M_{\text{min}}$.

The computational volume is divided into 1024^3 PM cells. We assume that dwarf galaxies form

in cells where the density ρ_X of background matter exceeds a threshold density $\rho_{\text{GF}} = \Delta_c \bar{\rho}(z)$, where $\bar{\rho}(z)$ is the mean density of the universe at redshift z , and $\Delta_c = 200$. We use the density of the background matter, and not the total density, because the matter already locked up in galaxies is unavailable to form new galaxies, except by mergers. We assume that in each cell that satisfies this criterion, there is a probability P of forming a dwarf galaxy of mass M_{min} during a time interval Δt , given by $P = \Psi \Delta t$, where Ψ is a galaxy formation rate. The number of galaxies created during a timestep is therefore

$$N_{\text{gal}} = \Psi N_{\text{cell}} \Delta t. \quad (2)$$

where N_{cells} is the number of cells that satisfy the criterion. We adjust the value of Ψ by requiring that the galaxy luminosity function at $z = 0$ is consistent with observations (see §3.1 below).

We select a subset of N_{gal} cells randomly among the N_{cell} cells that satisfy the criterion $\rho_X > \rho_{\text{GF}}$, and we create a galaxy of mass M_{min} in each of these cells. To do so, we consider a Gaussian density profile:

$$\rho(r) = \rho_{\text{GF}} e^{-r^2/2w^2}, \quad (3)$$

where r is the distance from the center of the cell, and the width w is defined by $(2\pi)^{3/2} \rho_{\text{GF}} w^3 = M_{\text{min}}$. This profile contains a total mass M_{min} . We identify all dark matter particles located within a distance $r = 4w$ from the center of the cell. We then remove from each particle a mass $\Delta m = C e^{-r^2/2w^2}$, where the constant C is adjusted such that the total mass removed is equal to M_{min} . Instead of locating the newborn galaxy in the exact center of the cell, we calculate the center-of-mass position and velocity of the matter that was removed from dark matter particles, and these become the position and velocity of the galaxy, respectively. This ensures that mass and momentum are conserved. The initial radius of the galaxy is set to $s = (3M_{\text{min}}/4\pi\rho_{\text{GF}})^{1/3}$, the radius of a uniform sphere with $M = M_{\text{min}}$ and $\rho = \rho_{\text{GF}}$.

For the simulation presented in this paper, we used a minimum mass $M_{\text{min}} = 2 \times 10^9 M_{\odot}$, which corresponds to the mass of 7 dark matter particles. The corresponding filter width is $w = 25.8 \text{ kpc}$, or 0.2645 PM cells.

2.3. The Subgrid Physics

Our treatment of subgrid physics is presented in Paper I, and we refer the reader to that paper for details. Here we briefly summarize the method used. At each timestep, we identify all pairs of galaxies that are sufficiently close that the center of one galaxy is inside the other galaxy, that is, $r_{ij} < \max(s_i, s_j)$, where r_{ij} is the separation between galaxies i and j , and s_i, s_j are their radii. For each pair, we calculate the total energy of the two galaxies in the center-of-mass frame,

$$E_{ij} = K_i + K_j + W_{ij} + U_i + U_j, \quad (4)$$

where K_i and K_j are the kinetic energy of galaxies i and j in the center-of mass frame, U_i and U_j are the internal energies of the galaxies, and $W_{ij} = -Gm_i m_j / r_{ij}$ is the gravitational potential energy of the galaxy pair, respectively. The internal energies depend on the masses and radii of the galaxies. They are given by

$$U_i = -\frac{\zeta G m_i^2}{2s_i}, \quad (5)$$

where m_i and s_i are the mass and radius of galaxy i , respectively. The *geometric factor* ζ depends on the density profile of the galaxy, but does not vary much for any reasonable profile, so, as in Paper I, we use $\zeta = 1$, which is the correct value for a truncated isothermal sphere in virial equilibrium.

If $E_{ij} < 0$, the merger criterion is satisfied and the two galaxies merge, to form a new galaxy k . The mass, position, velocity, and radius of that galaxy are initialized using:

$$m_k = m_i + m_j, \quad (6)$$

$$\mathbf{r}_k = \mathbf{r}_{ij}, \quad (7)$$

$$\mathbf{v}_k = \mathbf{v}_{ij}, \quad (8)$$

$$s_k = -\frac{\zeta G m_k^2}{2E_{ij}} = \frac{\zeta G m_k^2}{2|E_{ij}|}, \quad (9)$$

where \mathbf{r}_{ij} and \mathbf{v}_{ij} are the center-of-mass position and velocity, respectively. These equations ensure conservation of mass, momentum, and energy during mergers.

Tidal disruption is more tricky. When a galaxy is disrupted by the tidal field of a more massive one, the inner part of the galaxy might survive, while the outer part gets stripped. Some of the material stripped might then escape the system, or might get accreted by the massive galaxy. We simplify the problem by using an all-or-nothing approach. We identify pairs of galaxies which are sufficiently close that the separation between their *edges* is smaller than the radius of the largest galaxies, that is, $r_{ij} - s_i - s_j < \max(s_i, s_j)$. Let us assume that galaxy i is the most massive of the pair. We compare the tidal field of galaxy i at the location of galaxy j with the gravitational field of galaxy j itself. If we estimate that the tidal field is strong enough to unbind more than 50% of the mass of galaxy j , then the tidal disruption criterion is satisfied, and we assume that galaxy j is totally destroyed. Otherwise, galaxy j survives the encounter. In the case of a tidal destruction, we also check the merger criterion [eq. (4)]. If that criterion is also satisfied, we assume that galaxy j is destroyed by the tidal field of galaxy i , and then the fragments accrete onto galaxy i . Numerically this is treated as a merger. Galaxy particles being destroyed and not reaccreted are flagged, to indicate that they do not represent galaxies anymore but rather tidal fragments. They remain in the simulation, but are ignored during subsequent encounters. This enables us to track the motion of tidal fragments, and eventually determine in which cluster they end up (see § 3.3 below).

As we argue in Paper I, our treatment of mergers and tidal disruption would be too simplistic to describe individual events, but can be used to describe the net, collective effect of tens of thousands

of galactic encounters.

3. RESULTS

3.1. Galaxy Luminosity Function and Stellar Mass function

The simulation produces 79,751 galaxies with masses in the range $2 \times 10^9 M_\odot - 7.47 \times 10^{13} M_\odot$, including 251 objects with mass $M > 10^{12} M_\odot$. Clearly, such massive objects cannot be individual galaxies. We interpret them as individual subhalos hosting several galaxies, more specifically a *central galaxy* and one or several *satellite galaxies*. With this in mind, we can now calculate the luminosity function of galaxies. To convert masses into luminosities, we use the conditional luminosity function of Yang et al. (2003). The average number of galaxies in the luminosity interval $[L - dL/2, L + dL/2]$ hosted by a halo of mass M is given by

$$\phi(L|M) = \frac{\tilde{\phi}^*}{\tilde{L}^*} \left(\frac{L}{\tilde{L}^*} \right)^{\tilde{\alpha}} e^{-L/\tilde{L}^*}, \quad (10)$$

where $\tilde{\phi}^*$, \tilde{L}^* , and $\tilde{\alpha}$ are functions of the halo mass. The average mass-to-light ratio of halos is approximated by the following fitting formula:

$$\frac{M}{L} = \frac{1}{2} \left(\frac{M}{L} \right)_0 \left[\left(\frac{M}{M_1} \right)^{-\beta} + \left(\frac{M}{M_1} \right)^{\gamma_1} \right]. \quad (11)$$

If a halo hosts more than one galaxy, the mean luminosity of the most luminous galaxy is given by

$$\bar{L}_c(M) = \tilde{\phi}^* \tilde{L}^* \Gamma(\tilde{\alpha} + 2, L_1/\tilde{L}^*), \quad (12)$$

where Γ is the incomplete Gamma function, and L_1 is defined by

$$\tilde{\phi}^* \Gamma(\tilde{\alpha} + 1, L_1/\tilde{L}^*) = 1. \quad (13)$$

Note that there are more recent studies of the halo mass function and stellar mass function, from which the mass-to-light ratio can be calculated (Tinker et al. 2008; Behroozi et al. 2010). But these studies are limited to halos of mass $M > 10^{11} M_\odot$. The M/L ratio of Yang et al. (2003) covers the range $M = 10^9 h^{-1} M_\odot - 10^{14} h^{-1} M_\odot$, which is appropriate for our work. We used their model M1, defined by $M_1 = 10^{11.27} h^{-1} M_\odot$, $(M/L)_0 = 134 h M_\odot / L_\odot$, $\beta = 0.77$, $\gamma_1 = 0.32$.

Using equation (12), we calculated the central luminosity \bar{L}_c of each galaxy particle in the simulation. The resulting luminosity function is shown by the dotted histogram in the top panel of Figure 1. For comparison, the solid curve shows a Schechter luminosity function with $\phi^* = 1.61 \times 10^{-2} h^3 \text{Mpc}^{-3}$, $L^* = 9.64 \times 10^9 h^{-2} L_\odot$ and $\alpha = -1.21$ (Yang et al. 2003). There is an excellent

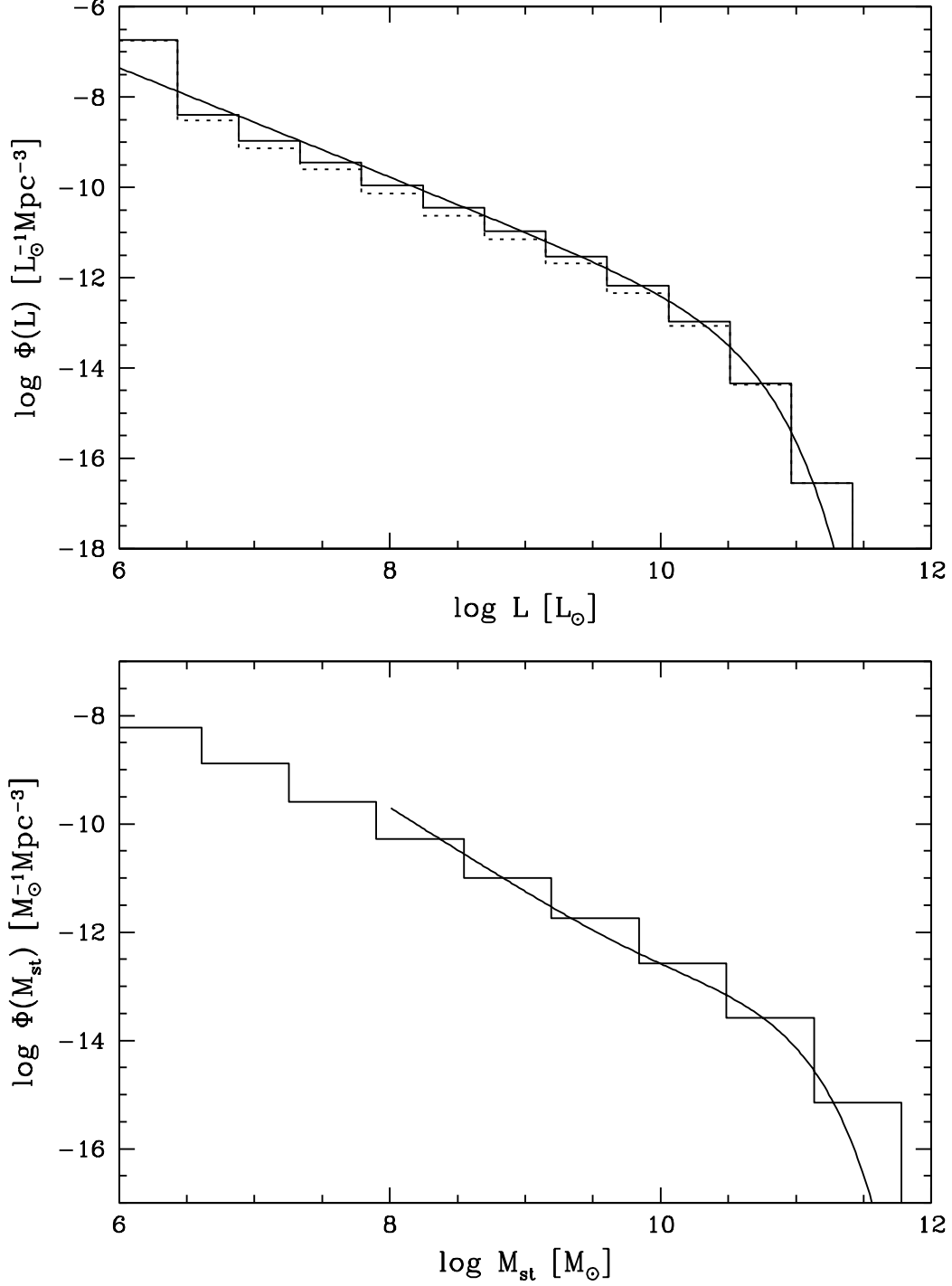


Fig. 1.— Top panel: Luminosity function of galaxies at $z = 0$. Dotted histogram: central galaxies only; solid histogram: all galaxies; solid curve: Schechter luminosity function with $\phi^* = 1.61 \times 10^{-2} h^3 \text{Mpc}^{-3}$, $L^* = 9.64 \times 10^9 h^{-2} L_\odot$ and $\alpha = -1.21$. Bottom panel: Stellar mass function of galaxies at $z = 0$. Histogram: all galaxies; solid curve: Stellar mass function of Baldry et al. (2008) (their eqs. [2]-[3]).

agreement at high luminosities, $L > 10^{10}L_{\odot}$. At lower luminosities, our simulated luminosity function is systematically below the Schechter function, except in the lowest bin where our results exceed the Schechter function by an order of magnitude. However, if we interpret galaxy particles of mass $M > 10^{12}M_{\odot}$ as actually being halos containing several galaxies, then equation (12) underestimates the total luminosity of these objects. By integrating equation (10), we can calculate the contribution of satellite galaxies in each luminosity bin, and include it in the luminosity function. The result is shown by the solid histogram in the top panel of Figure 1. There is now a good agreement with the Schechter function at all luminosities $L > 10^{8.5}L_{\odot}$, while there is still a mismatch at lower luminosities. We attribute this to the discreteness of the algorithm, in which all galaxy masses are multiples of M_{\min} . In particular, the three lowest luminosity bins in Figure 1 contain, respectively, galaxies of mass M_{\min} , of mass $2M_{\min}$, and of masses $3M_{\min}$ and $4M_{\min}$. We can understand the large excess in the lowest luminosity bin by noting that galaxies of mass M_{\min} are allowed to form directly, while more massive galaxies must be built-up through a series of mergers.

We find this agreement quite remarkable. There is nothing in our galaxy formation algorithm that guaranties a priori that the final luminosity function would even resemble a Schechter function. The model was never tuned to obtain this result, and there is not much that *could* be tuned. We use a density threshold of $200\bar{\rho}$ for identifying collapsed objects, which is a standard value based on theoretical arguments.¹ The geometric factor ζ entering into the merger criterion is a free parameter, but its value is close to unity for any reasonable density profile. We argue that the features seen in the simulated luminosity function at low luminosities are caused by the discreteness of the galaxy masses. Hence, using a different value of M_{\min} would most likely move these features to different luminosities without affecting the high-end of the luminosity function. The only real free parameter in our model is the galaxy formation rate Ψ . Changing that parameter might improve the fit at low luminosities, at the cost of worsening it at high luminosities. Overall, we find that our model provides a satisfactory fit to the Schechter luminosity function. In particular, it correctly predicts the value of the luminosity break L_* , though that value (or the corresponding mass M_*) is not built-in in the model.

Since the M vs L relation is non-linear, when two galaxies merge, the merger remnant does not have the total luminosity of the two progenitors. This simply reflects the fact that galactic evolution is much more than just a series of mergers. The luminosity of galaxies is affected by processes such as star formation and evolution, accretion, galactic winds, AGN activity, and so on. Since these processes are not included in our model, we cannot predict the evolution of the luminosities of galaxies during and between mergers. This is why we calculate the values of the luminosity using the observed M vs. L relation.

Once we have the luminosities, we can easily estimate the stellar masses. We use the relation given by Bell et al. (2003) for g-band luminosities: $\log_{10}(M_{\text{st}}/L) = -2.61 + 0.998 \log_{10} M_{\text{st}} h^2$, where the stellar mass M_{st} and luminosity L are in solar units. For a cosmological model with $h = 0.704$,

¹This is an approximation to $18\pi^2$, the exact value for a spherical collapse in a $\Omega_0 = 1$ universe.

this reduces to $M_{\text{st}} = 0.000142L^{1.425}$. The resulting galactic stellar mass function is shown by the histogram in the bottom panel of Figure 1. For comparison, we show the observed stellar mass function of Baldry et al. (2008), which covers the stellar mass range $M_{\text{st}} = 10^8 - 10^{12}M_{\odot}$. There is an excellent agreement over the range of masses covered by the observations, except possibly at the highest mass bin.

3.2. Global Properties

Figure 2 shows the cumulative number of mergers, of tidal destruction events with the tidal fragments dispersed in the intracluster space, and of tidal destruction events followed by accretion of the fragments onto the massive galaxy (these cases are also counted as mergers). The number of all types of events increase roughly exponentially with redshift. The delay between the start of merger events ($z = 5.9$) and tidal destruction events ($z = 4.8$) reflects the time it takes to build galaxies of different masses, an essential condition for tidal destruction. At redshifts $z > 1$, more than 90% of tidal destruction events result in the fragments being dispersed into the intracluster space, and therefore contributing to the ICL. After $z = 1$, accretion of tidal fragments by the massive galaxy becomes more common, and dominates after $z = 0.5$.

Figure 3 shows the mass of the galaxies involved in tidal destruction followed by dispersion, with m_1 being the mass of the galaxy being destroyed, and m_2 being the mass of the other, more massive galaxy. The most striking feature is that tidal destruction is not limited to dwarf galaxies, but covers more than three orders of magnitudes in mass. The most massive galaxy destroyed had a total mass $m_1 = 1.29 \times 10^{13}M_{\odot}$, and was destroyed by a galaxy of mass $m_2 = 2.20 \times 10^{13}M_{\odot}$ at redshift $z = 0.48$. Figure 4 shows a similar plot, for all merger events (direct mergers, and tidal destruction followed by accretion). There are noticeable differences. First, the top left corner of the plot is populated, showing that encounters with very large mass ratios ($m_2/m_1 > 2500$) never result in dispersion, but can result in mergers. Second, there is a clear “desert” in Figure 4 at masses $m_1 > 3 \times 10^{11}M_{\odot}$ (or $M_{\text{st}} > 5 \times 10^9M_{\odot}$), between mass ratios $m_2/m_1 = 1$ and 10, which is not found in Figure 3. To investigate this, we focus on encounters with $m_1 > 3 \times 10^{11}M_{\odot}$, and combine the two figures. The results are shown in Figure 5, where we use different symbols for direct mergers, tidal destruction followed by dispersion, and tidal destruction followed by accretion. There is a remarkable separation between the three processes. Direct mergers occur at low mass ratios, $m_2/m_1 < 1.2$, dispersion occurs mostly at intermediate ratios, $1.2 < m_2/m_1 < 10$, and accretion occurs mostly at high mass ratio, $m_2/m_1 > 10$. To explain these results, let us consider what happens, in the simulation, during an encounter between a galaxy of mass m_1 and size s_1 and a galaxy of mass $m_2 > m_1$ and size s_2 , separated by a distance r_{12} . The tidal disruption and merger criteria used in our model will determine the outcome of this encounter. The gravitational field that binds the first galaxy is of order $E \sim Gm_1/s_1^2$, while the tidal field of the second galaxy at the location of the first one is of order $T \sim Gm_2s_1/r_{12}^3$. The ratio of these fields, T/E is then proportional to $(m_2/m_1)(s_1/r_{12})^3$. Since $s_1 < r_{12}$, it takes a certain mass ratio for tidal destruction

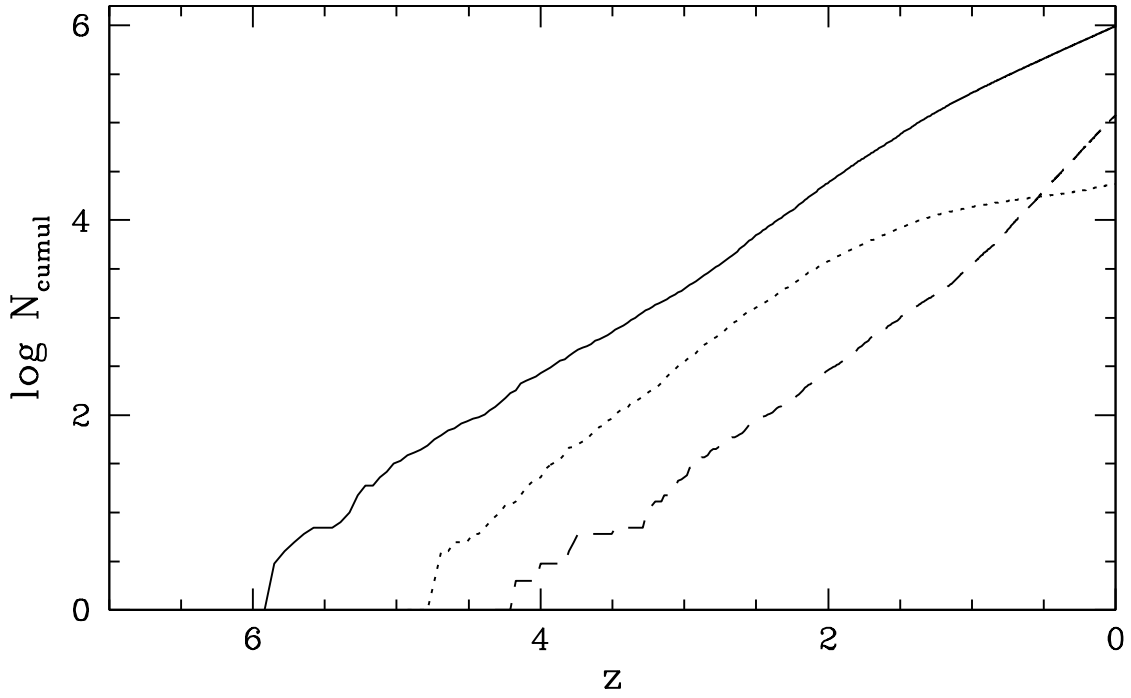


Fig. 2.— Cumulative number of mergers (solid line), tidal destruction events, with fragments dispersed in the intracluster space (dotted line), and tidal destruction events followed by accretion of the fragments onto the massive galaxy (dashed line), versus redshift.

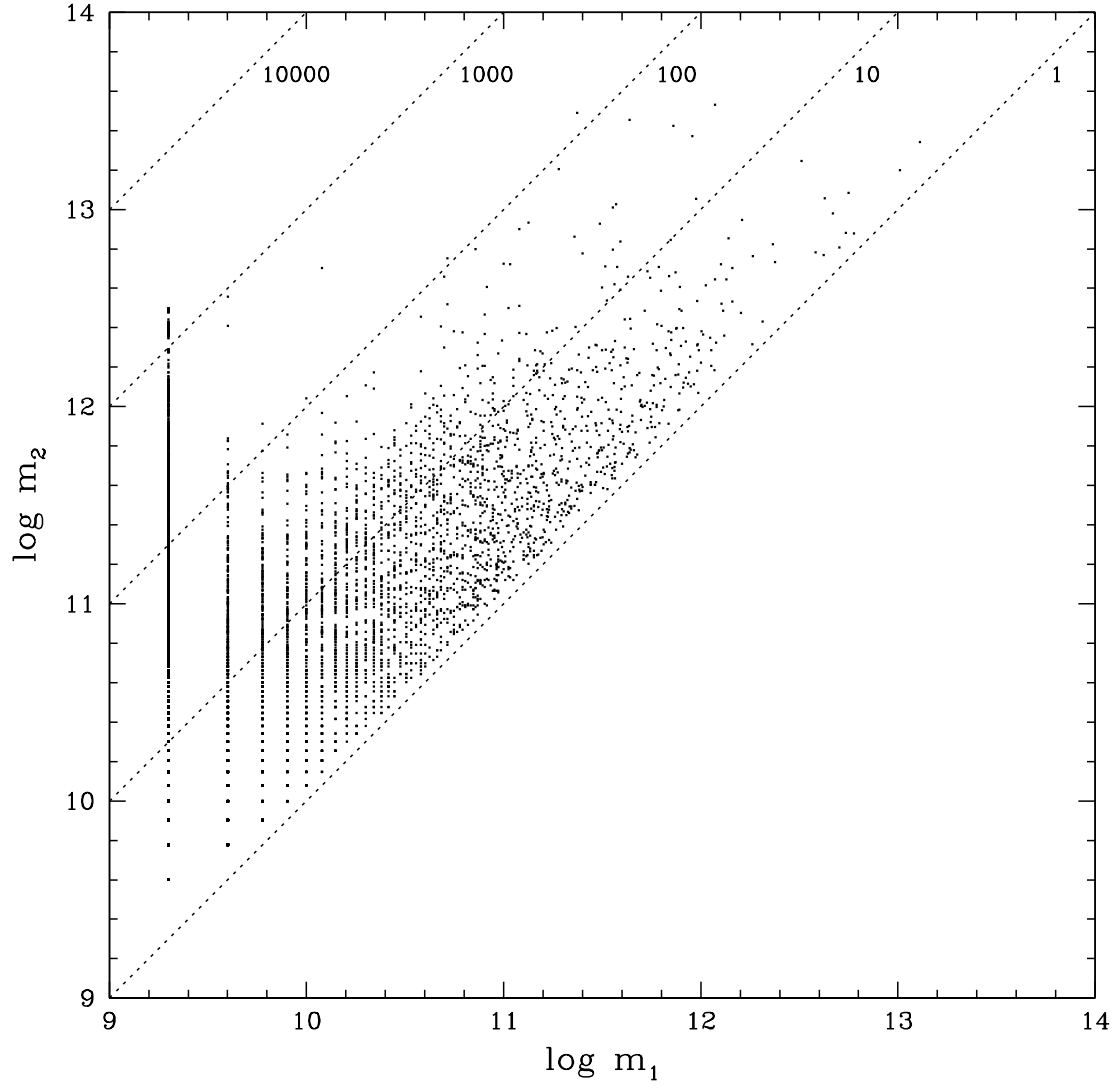


Fig. 3.— Encounters resulting in tidal destruction, with dispersion of the fragments. m_1 and m_2 are the mass of the lower- and higher-mass galaxies, respectively. Dashed lines indicate mass ratios.

to occur. Hence, encounters between galaxies of comparable masses can only result in either mergers (solid circles in Fig. 5) or nothing. But if the mass ratio is sufficiently large for the tidal disruption criterion to be satisfied, the lower-mass galaxy will be destroyed, and the merger criterion will determine whether the fragments are dispersed, or accreted by the higher-mass galaxy. Unlike the tidal disruption criterion, the merger criterion depends on the velocity of the galaxies [K -terms in eq. (4)]. High-mass galaxies tend to be located in massive clusters. Their velocities are usually not determined by their properties and the ones of their immediate neighbors, but rather by the overall properties of the cluster in which these galaxies are located. In particular, we expect the velocity of a galaxy orbiting inside a cluster to be of order the velocity dispersion at its location, independently of its mass or the mass of its neighbors. We can then rewrite equation (4) as

$$E_{12} \approx \frac{m_1 \sigma^2}{2} + \frac{m_2 \sigma^2}{2} - \frac{Gm_1 m_2}{r_{12}^2} - \frac{\zeta G m_1^2}{s_1} - \frac{\zeta G m_2^2}{s_2}, \quad (14)$$

where σ is the local velocity dispersion. If m_1 and m_2 are small, the kinetic energy terms will dominate, and the criterion will fail ($E_{12} > 0$). The galaxies will simply pass by each other without merging, and if the tidal disruption criterion is satisfied (notice that it does not depend on velocities), the lower-mass galaxy will be destroyed and the fragments will be dispersed (crosses in Fig. 5). If we then keep m_1 constant and increase m_2 , the second, third, and fifth terms in equation (14) will increase in amplitude. With two of these terms being negative, and the last one being quadratic in m_2 , E_{12} will decrease, and for high enough values of m_2 , the criterion $E_{12} < 0$ will be satisfied. The galaxies will merge, and since increasing m_2 while keeping m_1 constant also favors the tidal disruption criterion, the outcome will be tidal destruction followed by reaccretion of the fragments (open circles in Fig. 5).

Figures 6 and 7 show the properties of the galaxies that are tidally destroyed, with fragments dispersed into the intracluster space, as functions of the galaxies' total mass m_1 (Fig. 6) and stellar mass M_{st} (Fig. 7). The top panels show the number of galaxies destroyed in different mass bins. Most galaxies destroyed are low-mass galaxies: 89.8% of galaxies destroyed have masses $m_1 < 10^{10} M_\odot$, $M_{\text{st}} < 2.8 \times 10^6 M_\odot$, while only 0.16% have masses $m_1 > 10^{12} M_\odot$, $M_{\text{st}} > 3 \times 10^{10} M_\odot$. The middle panels show the total mass and total stellar mass in each mass bin. The contribution of low-mass galaxies is very small. 42.1% of the mass in tidal fragments comes from galaxies in the range $m_1 = 10^{11} - 10^{12} M_\odot$ and $M_{\text{st}} = 6 \times 10^8 - 3 \times 10^{10} M_\odot$. The peak at $m_1 = M_{\text{min}} = 2 \times 10^9 M_\odot$ results from the fact that there are too many galaxies of that mass to start with, as we explained in § 3.1. Using equation (11), we calculated the total luminosity in each mass bin. The resulting distribution is plotted in the bottom panels of Figures 6 and 7. 57.9% of the ICL comes from galaxies in the range $m_1 = 10^{11} - 10^{12} M_\odot$, $M_{\text{st}} = 6 \times 10^8 - 3 \times 10^{10} M_\odot$, 30.6% from massive, $m_1 > 10^{12} M_\odot$, $M_{\text{st}} > 3 \times 10^{10} M_\odot$ galaxies, and only 11.5% from low-mass, $m_1 < 10^{11} M_\odot$, $M_{\text{st}} < 6 \times 10^8 M_\odot$ galaxies, including 1.0% from $m_1 < 10^{10} M_\odot$, $M_{\text{st}} < 2.8 \times 10^6 M_\odot$ galaxies. Willman et al. (2004) also found that intermediate-mass galaxies were an important contributor to the ICL.

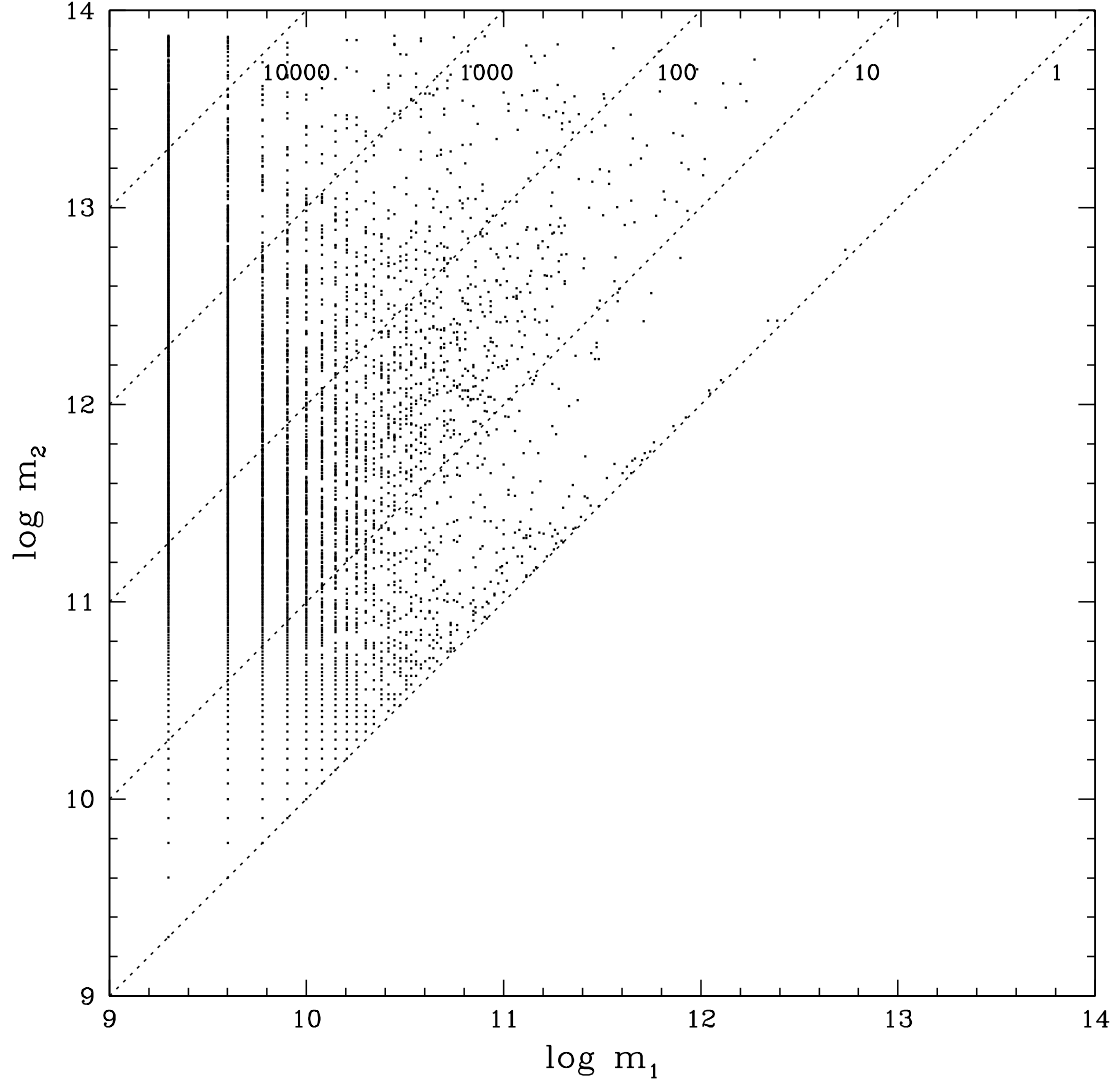


Fig. 4.— Encounters resulting in mergers (including tidal destruction followed by accretion). m_1 and m_2 are the mass of the lower- and higher-mass galaxies, respectively. Dashed lines indicate mass ratios.

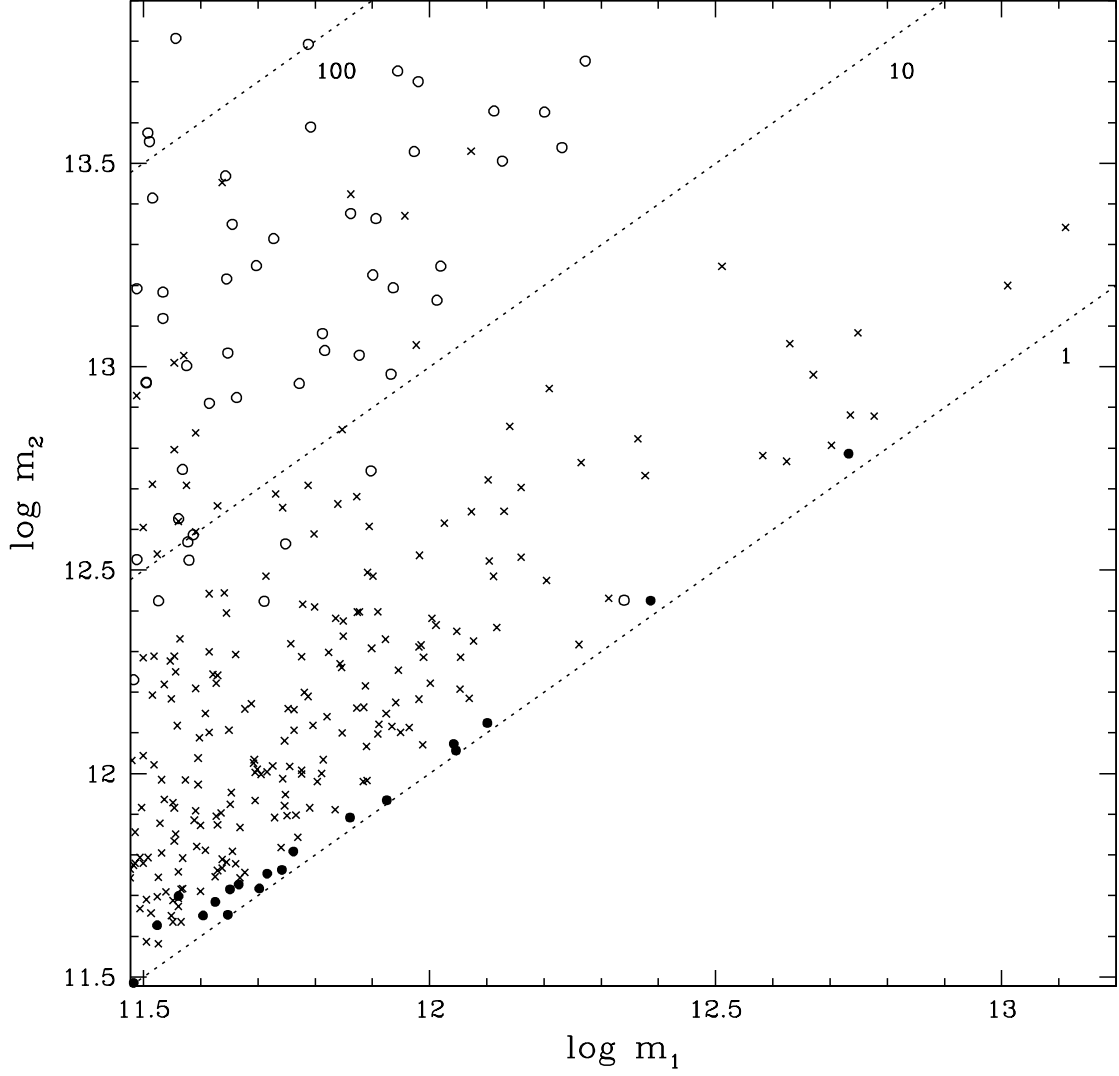


Fig. 5.— Encounters involving galaxies with masses $m > 3 \times 10^{11} M_{\odot}$. m_1 and m_2 are the mass of the lower- and higher-mass galaxies, respectively. Solid circles: direct mergers; crosses: tidal destruction with fragments dispersed into the intracluster space; open circles: tidal destruction followed by accretion. Dashed lines indicate mass ratios.

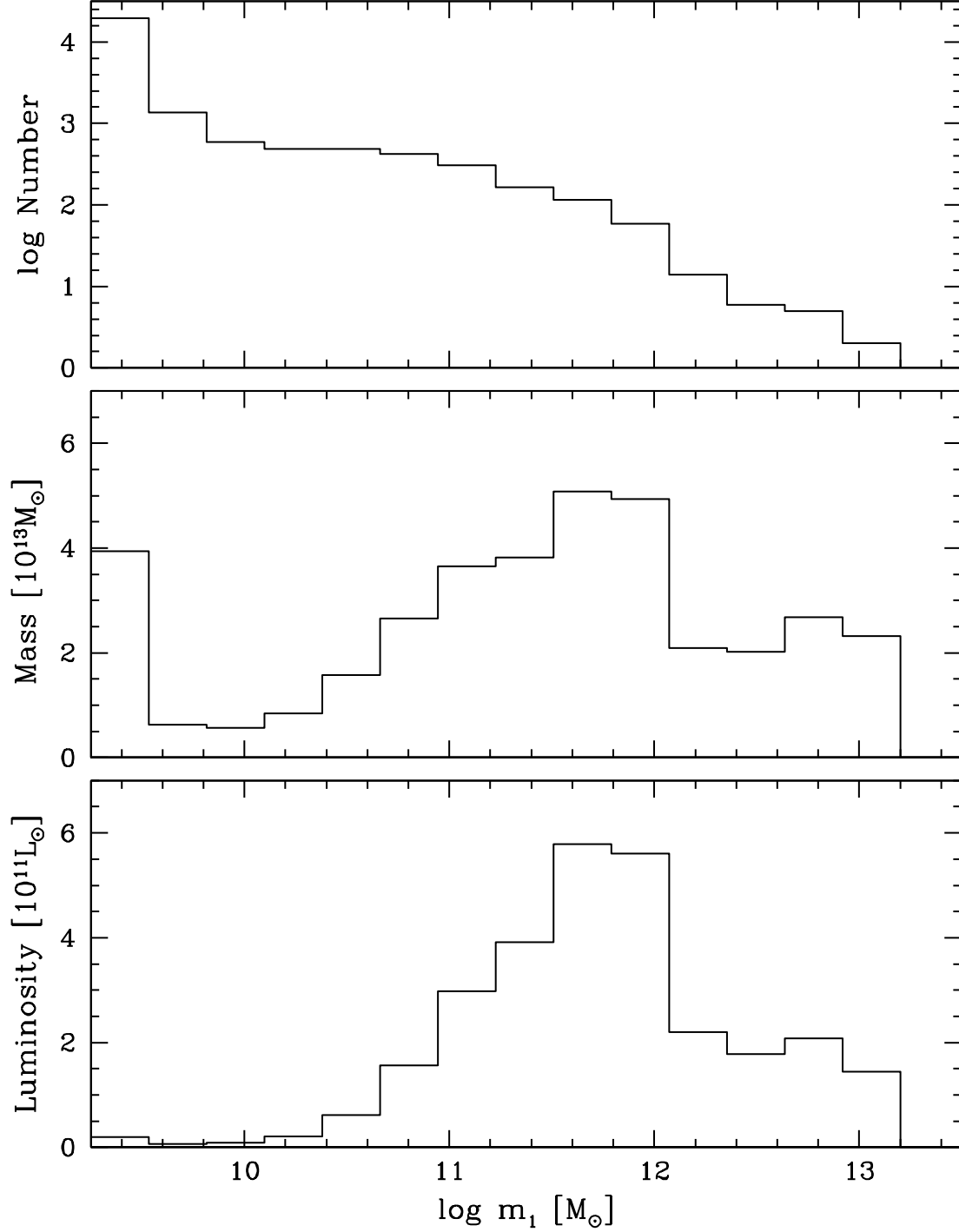


Fig. 6.— Properties of tidally destroyed galaxies which contribute to the ICL, versus mass. Top panel: number of galaxies in each mass bin; middle panel: total mass in each mass bin; bottom panel: total luminosity in each mass bin.

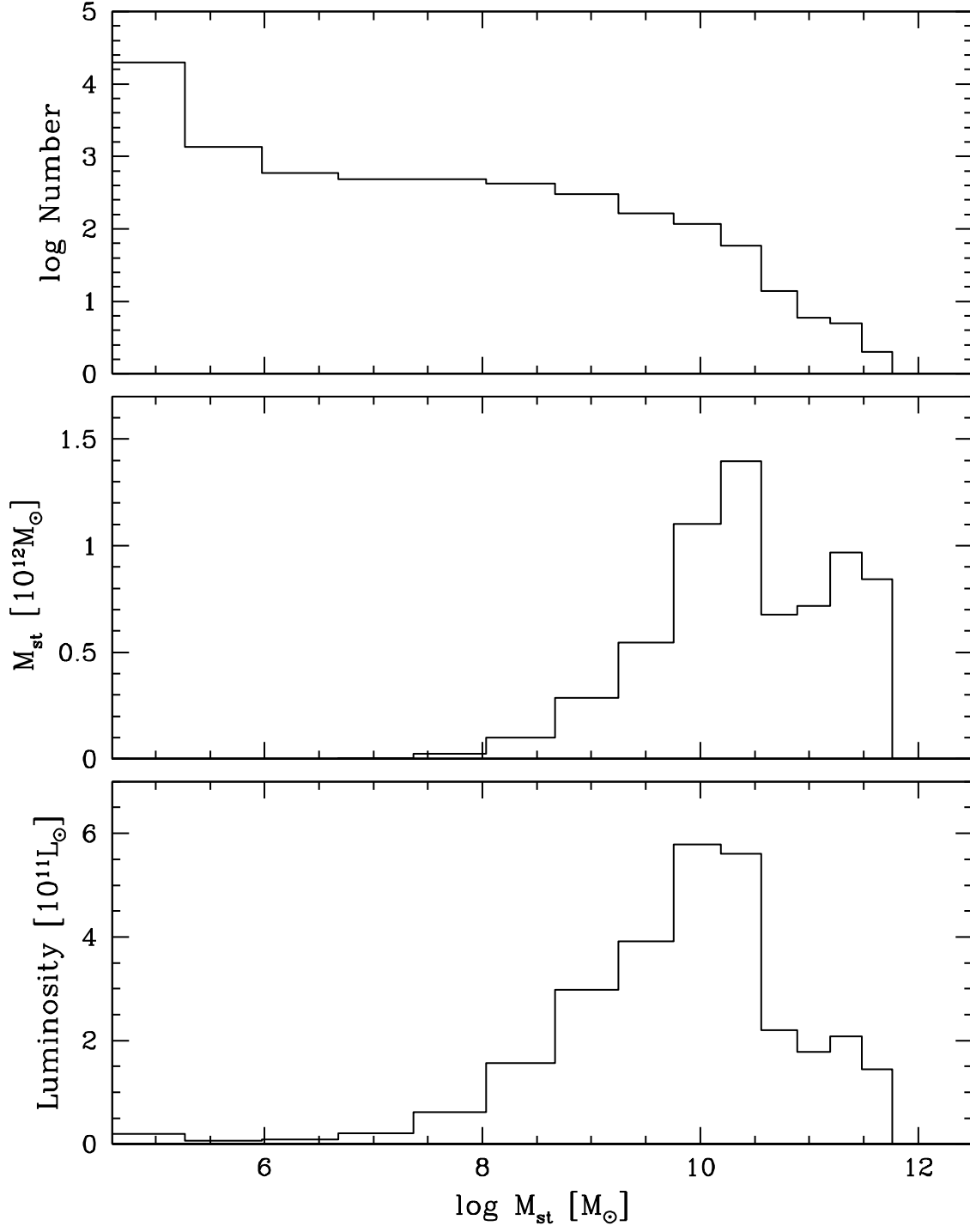


Fig. 7.— Properties of tidally destroyed galaxies which contribute to the ICL, versus stellar mass. Top panel: number of galaxies in each mass bin; middle panel: total stellar mass in each mass bin; bottom panel: total luminosity in each mass bin.

3.3. Cluster Analysis

3.3.1. Intracluster Light Fraction

We identify clusters using a standard friends-of-friends algorithm (FOF) with a linking length equal to 0.25 times the mean particle spacing (corresponding to 48.8 kpc comoving). This algorithm identifies the dark matter particles, galaxies, and tidal fragments that belong to each cluster. The term *tidal fragment* refers here to galaxies that have been flagged as being tidally destroyed, with their fragments dispersed into the intracluster space. At $z = 0$, we find 18 massive clusters, with masses $M_{\text{cl}} > 10^{14} M_{\odot}$. For each galaxy and tidal fragment located in these clusters, we calculate the luminosity using equation (11). By adding these luminosities, we get the total galaxy luminosity L_{gal} and the total intracluster luminosity L_{ICL} for each cluster. The properties of the clusters are listed in Table 1. M_{cl} , M_{gal} , and M_{tid} are the total mass of the cluster, the mass in galaxies, and the mass in tidal fragments, respectively. L_{gal} and L_{ICL} are the galaxy and intracluster luminosity, respectively, and $f_{\text{ICL}} \equiv L_{\text{ICL}} / (L_{\text{gal}} + L_{\text{ICL}})$ is the fraction of intracluster light.

The values of f_{ICL} vary from 1% to 58%, while observed values vary from 1.6% to 50% (see Table 12 of Paper I). Our simulations therefore reproduce the range of observed values of f_{ICL} . However, we only have 4 clusters (out of 18) with $f_{\text{ICL}} < 20\%$, while such low values are more common among observed clusters. Rudick et al. (2011) simulated 6 clusters, and found values of f_{ICL} in the range 9% – 36%. Most of their simulated clusters have $f_{\text{ICL}} < 20\%^2$. Henriques et al. (2008) report median values of $f_{\text{ICL}} = 20\%$ for halos with masses $M_{\text{cl}} \sim 10^{13} h^{-1} M_{\odot}$ and $f_{\text{ICL}} = 30\%$ for halos with masses $M_{\text{cl}} \sim 10^{15} h^{-1} M_{\odot}$. Visual inspection of their Figure 6 indicates values of f_{ICL} in the range 10% – 50% for the mass range $M_{\text{cl}} > 10^{14} M_{\odot}$ we consider. Overall, there is a broad agreement between the values of f_{ICL} obtained by us, by Rudick et al. (2011), by Henriques et al. (2008), and the observed values. The ranges of values are very wide. In § 3.3.3 below, we investigate the physical origin of this, and argue that it is a consequence of the hierarchical formation of clusters.

Figure 8 shows the dependencies of cluster properties on the total mass of the cluster. The top left panel shows the mass fraction in galaxies and tidal fragments. There is a lot of scatter, but overall the mass fraction is around 0.08 for galaxies and 0.03 for tidal fragments, with $M_{\text{gal}} > M_{\text{tid}}$ for all clusters. The top right panel shows the stellar masses $M_{\text{st,gal}}$ and $M_{\text{st,ICS}}$ in galaxies and intracluster stars, and the bottom left panel shows the luminosities L_{gal} and L_{ICL} . All these quantities increase roughly linearly with M_{cl} . Most of the light comes from the galaxies, with two notable exceptions: clusters C01 (the most massive one) and C05. The bottom right panel shows the intracluster light fraction f_{ICL} . There is no obvious correlation with cluster mass, except for the fact that massive clusters tend to have large values of f_{ICL} , with 4 of the 5 most massive clusters having $f_{\text{ICL}} \leq 40\%$, while only 2 of the least 13 massive ones have values of f_{ICL} this high. Some studies have found no significant dependence of f_{ICL} on cluster mass (Dolag et al. 2010; Puchwein et al.

²Each cluster in the simulations of Rudick et al. (2011) has several values of f_{ICL} because they experiment with various techniques for calculating that quantity.

Table 1. Properties of Massive Clusters

| Name | $M_{\text{cl}} [10^{14} M_{\odot}]$ | $M_{\text{gal}} [10^{14} M_{\odot}]$ | $M_{\text{tid}} [10^{14} M_{\odot}]$ | $L_{\text{gal}} [10^{11} L_{\odot}]$ | $L_{\text{ICL}} [10^{11} L_{\odot}]$ | $f_{\text{ICL}} [\%]$ |
|------|-------------------------------------|--------------------------------------|--------------------------------------|--------------------------------------|--------------------------------------|-----------------------|
| C01 | 12.16 | 0.869 | 0.539 | 3.887 | 4.207 | 52 |
| C02 | 10.28 | 0.914 | 0.313 | 3.289 | 2.151 | 40 |
| C03 | 5.62 | 0.573 | 0.110 | 2.804 | 0.879 | 24 |
| C04 | 5.40 | 0.369 | 0.223 | 2.156 | 1.866 | 46 |
| C05 | 3.34 | 0.228 | 0.169 | 1.071 | 1.504 | 58 |
| C06 | 2.98 | 0.315 | 0.037 | 1.916 | 0.256 | 12 |
| C07 | 2.52 | 0.204 | 0.096 | 1.279 | 0.813 | 39 |
| C08 | 2.02 | 0.192 | 0.045 | 1.204 | 0.401 | 25 |
| C09 | 1.94 | 0.187 | 0.041 | 1.236 | 0.317 | 20 |
| C10 | 1.71 | 0.130 | 0.072 | 1.019 | 0.668 | 40 |
| C11 | 1.63 | 0.146 | 0.040 | 1.077 | 0.351 | 25 |
| C12 | 1.36 | 0.094 | 0.066 | 0.719 | 0.644 | 47 |
| C13 | 1.23 | 0.124 | 0.021 | 0.795 | 0.162 | 17 |
| C14 | 1.21 | 0.105 | 0.032 | 0.828 | 0.277 | 25 |
| C15 | 1.13 | 0.103 | 0.033 | 0.669 | 0.312 | 32 |
| C16 | 1.11 | 0.117 | 0.003 | 0.745 | 0.006 | 1 |
| C17 | 1.09 | 0.108 | 0.012 | 0.702 | 0.087 | 11 |
| C18 | 1.06 | 0.162 | 0.053 | 1.234 | 0.497 | 29 |

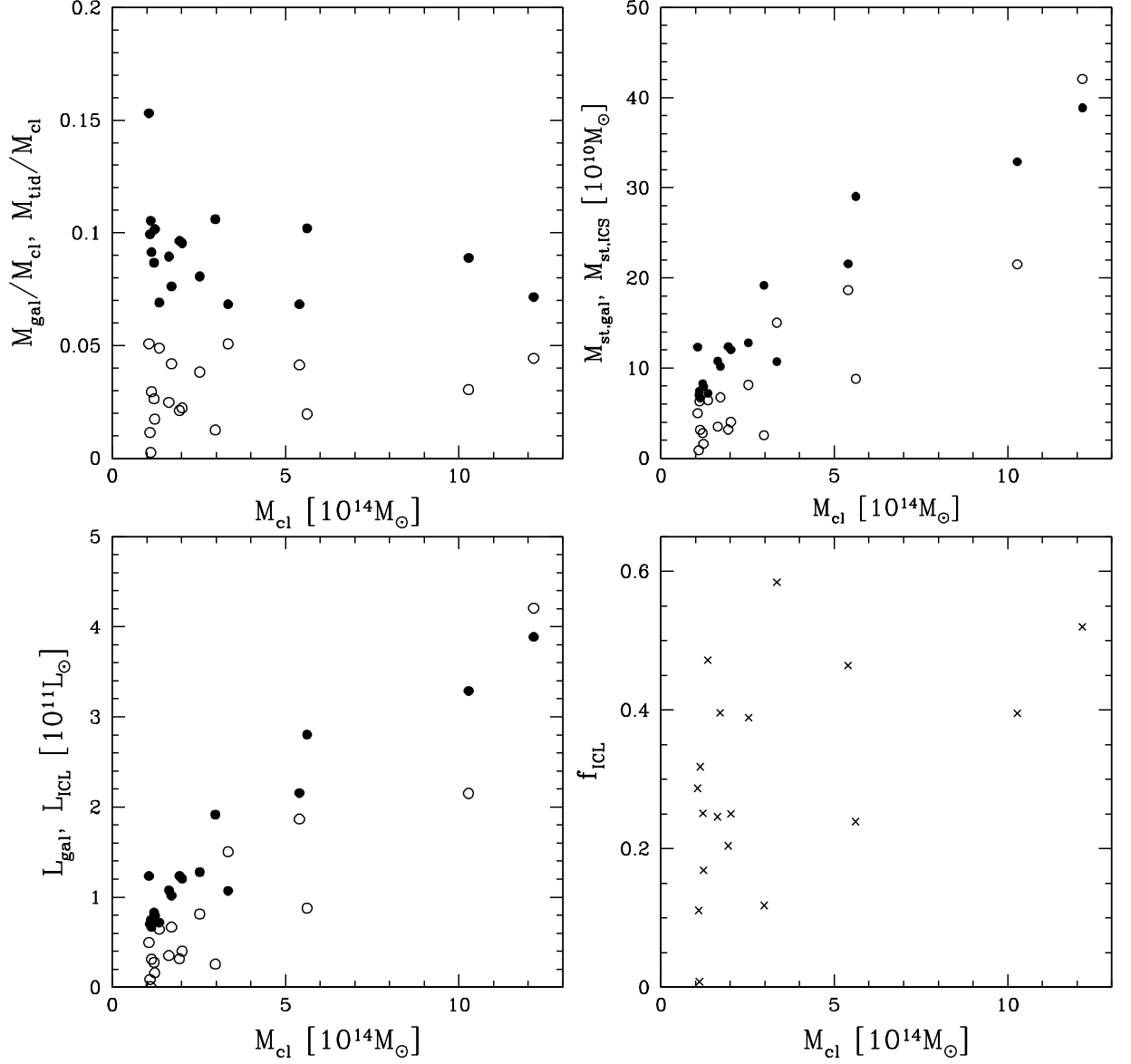


Fig. 8.— Top left panel: fraction of cluster mass inside galaxies (solid circles) and inside tidal fragments (open circles) versus cluster mass. Top right panel: galaxy stellar mass (solid circles) and intracluster stellar mass (open circles) versus cluster mass. Bottom left panel: galaxy luminosity (solid circles) and intracluster luminosity (open circles) versus cluster mass. Bottom right panel: intracluster light fraction versus cluster mass.

2010; Rudick et al. 2011), while others found that f_{ICL} tends to increase with M_{cl} (Purcell et al. 2007; Murante et al. 2007; Henriques et al. 2008). Our results are somehow intermediate. We do not find very massive clusters with low f_{ICL} , but we do find some less-massive clusters with high f_{ICL} .

3.3.2. Cluster Evolution

We used our FOF algorithm to build clusters catalogs at various redshifts, and combined these catalogs to build merger trees for all 18 massive clusters found at $z = 0$. We then traced the ancestry of each cluster back in time, following the most massive progenitor. Figure 9 shows the evolution of the galaxy luminosity L_{gal} , intracluster luminosity L_{ICL} , and intracluster light fraction f_{ICL} , for a subset of 4 clusters. L_{ICL} increases with time as galaxies get tidally destructed. It could only decrease if tidal fragments were ejected from the clusters, but this does not seem to ever happen. L_{gal} is affected by several processes. Galaxy formation increases L_{gal} , while tidal destruction followed by dispersal decreases it. Galaxy merger events, and tidal destruction followed by accretion, both replace two galaxies by one with the same total mass. Since L does not vary linearly with M , the new galaxy does not have the total luminosity of its two progenitors, as we explained in §3.1. Overall, the values of f_{ICL} tend to increase with time, in agreement with the results of Rudick et al. (2011). However, there can be sudden drops in the value of f_{ICL} , such as the one seen at $t/t_0 = 0.6$ in cluster C04. These drops are caused by major cluster mergers. When two clusters of comparable masses, but with very different values of f_{ICL} , merge, the merger remnant will have a value of f_{ICL} that is intermediate between the values for the progenitors. If the progenitor with the largest value of f_{ICL} was identified as the main progenitor, then the net effect of the merger is to decrease f_{ICL} for that cluster. To illustrate this, we show in Figure 10 the merger tree for cluster C04. Though the cluster was built mostly through a series a minor merger (where one progenitor provides 80% or more of the mass), we see that a major merger took place between redshifts $z = 0.70$ and 0.49 . The main progenitor has a value $f_{\text{ICL}} = 0.46$, but provides only 38% of the mass. The next three progenitors all have lower values of f_{ICL} , and together provide 41% of the mass. As a result, the value of f_{ICL} drops from 0.46 to 0.29. A similar thing happens at $t/t_0 = 0.95$ for cluster C08. In the cases of clusters C01 and C14, we found that the late drop in f_{ICL} was not caused by a major merger, but rather by a sudden increase in galaxy formation.

These results are consistent with the results of Rudick et al. (2011). Their simulations show that f_{ICL} does not increase at a constant rate, and does not always vary monotonically.

3.3.3. The Range of Intracluster Light Fractions

Once the merger trees of clusters are built, we can investigate the origin of the very wide range in the values of f_{ICL} (from 1% to 58% in our simulation, and a comparable range in the observed

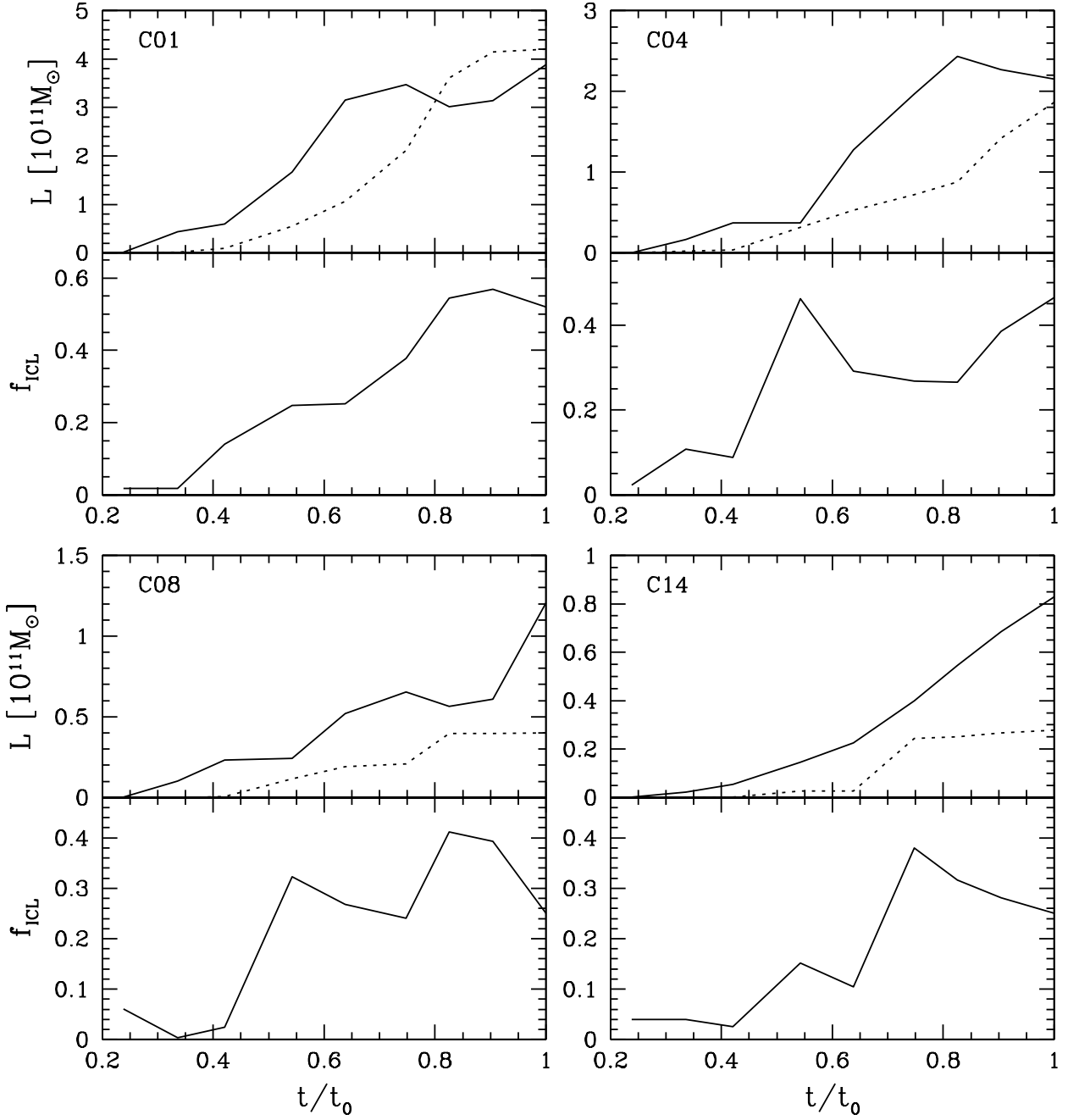


Fig. 9.— Time-evolution of the galaxy luminosity (top panels, solid curves), intracluster luminosity (top panels, dotted curves), and intracluster light fraction f_{ICL} (bottom panels), for clusters C01, C04, C08, and C14. t_0 is the present age of the universe.

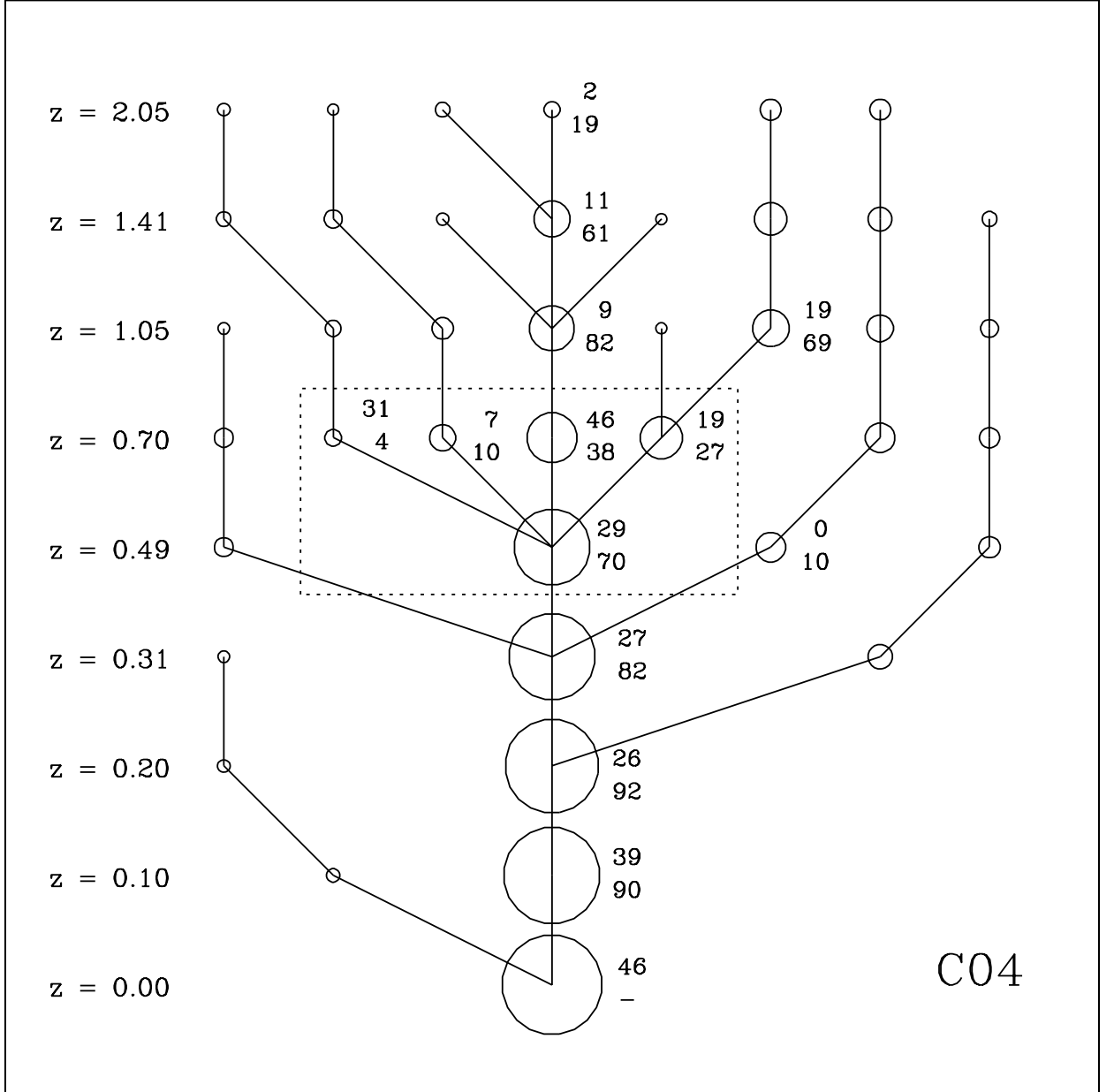


Fig. 10.— Merger tree for cluster C04. The area of each circle is proportional to the mass of the cluster. The numbers next to some clusters indicate the value of f_{ICL} in percentage (top), and the relative contribution of that cluster to the mass of the merger remnant, also in percentage (bottom). The dotted box indicates a major merger, where the most massive progenitor contributes only 38% of the final mass of the merger remnant. Redshifts are shown on the left. For clarity, only clusters with 20,000 particles or more are shown.

Table 2. Main Ancestry of Massive Clusters

| Name | f_{ICL} [%] | $z = 0.10$ | 0.20 | 0.31 | 0.49 | 0.70 | 1.05 | 1.41 | 2.06 |
|------|----------------------|------------|------|------|------|------|------|------|------|
| C01 | 52 | 90 | 90 | 86 | 80 | 57 | [35] | 79 | [22] |
| C02 | 40 | 89 | 92 | 87 | 78 | 84 | [35] | 80 | [31] |
| C04 | 46 | 90 | 92 | 82 | 70 | [38] | 82 | 61 | [19] |
| C05 | 58 | 92 | 93 | 90 | 81 | 87 | [46] | [32] | [29] |
| C07 | 39 | 79 | 91 | 88 | 75 | 83 | 70 | [33] | 69 |
| C08 | 25 | 64 | 90 | 92 | 87 | 57 | 80 | [45] | 71 |
| C10 | 40 | 91 | 91 | 73 | [48] | 53 | 67 | 66 | [43] |
| C12 | 47 | 90 | 92 | 83 | [45] | [48] | 67 | 63 | ... |
| C14 | 25 | 90 | 87 | 85 | [41] | 75 | [47] | 51 | 71 |
| C03 | 24 | 88 | 90 | 88 | 63 | 80 | 53 | 75 | [18] |
| C06 | 12 | 89 | 90 | 70 | 81 | 84 | 64 | 77 | 55 |
| C09 | 20 | 89 | 52 | 90 | 80 | 85 | 63 | 73 | [25] |
| C11 | 25 | 89 | 87 | 56 | 84 | 83 | 70 | 73 | [26] |
| C13 | 17 | 92 | 73 | 85 | 81 | 76 | 75 | 73 | 57 |
| C15 | 32 | 92 | 87 | 91 | 84 | 69 | 77 | 69 | [27] |
| C16 | 1 | 89 | 91 | 86 | 85 | 82 | 71 | 76 | 74 |
| C17 | 11 | 86 | 90 | 89 | 81 | 84 | 69 | 74 | [30] |
| C18 | 29 | 87 | 69 | 91 | 88 | 68 | 83 | 52 | 54 |

values). For each cluster, we started at redshift $z = 0$, and followed the ancestry back in time along the main progenitors. The results are shown in Table 2. For each cluster, we indicate, at each redshift $z > 0$ the contribution in percentage of that cluster to the mass of the merger remnant at the next redshift (the reader will recognize, for cluster C04, the numbers plotted along the central line in Fig. 10). We indicated in boldface and square brackets the major mergers, when less than 50% of the mass of the merger remnant comes from the main progenitor. We also separated the clusters in two groups (top and bottom). The clusters in the top group all experienced a major merger at intermediate redshift $z < 1.41$. The clusters in the bottom group experienced no major merger, or a major merger at high redshift. There is a striking correlation between the presence of major mergers at intermediate redshifts and the final value of f_{ICL} . All clusters in the top group have $f_{\text{ICL}} \geq 25\%$, and the seven highest values of f_{ICL} are found in that group; all clusters in the bottom group have $f_{\text{ICL}} \leq 32\%$, and the six lowest values of f_{ICL} are found in that group. Clearly, major mergers at intermediate redshift drive the evolution of f_{ICL} and determine the final value of $z = 0$. While minor mergers will tend to leave clusters essentially undisturbed, major mergers can have dramatic effects. In particular, the merger of two clusters of comparable masses, which contain comparable numbers of galaxies, can lead to a sudden increase in the number of density of galaxies. Since the frequency of encounters scales like the square of that number density, we expect a significant increase in the rate of encounters immediately after a major merger, and that rate might remain high all the way to $z = 0$. This will result in a large number of tidal destruction events, and a correspondingly high value of f_{ICL} . Notice that major mergers of clusters at $z = 2.06$ and do not have much effect, because the clusters do not contain many galaxies at that time.

This result is not at odds with the conclusion of the previous section. A major merger between clusters of comparable masses and different values of f_{ICL} can lead to a sudden drop in the value of f_{ICL} , depending on which progenitor is identified as the main one. But this sudden drop can be more than compensated by the increase rate of encounters that take place after the merger and can last all the way to the present. Cluster C04 provides a good illustration of this. f_{ICL} drops from 46% to 29% during the major merger, but is back at 46% by $z = 0$.

3.3.4. Projected Luminosity Distribution

Figure 11 shows the structure of some of the clusters. The greyscale images show the projected surface density of dark matter. The yellow and orange dots show the galaxies and tidal fragments, respectively. Some clusters, like C05 and C13, are relaxed objects with a well-defined core where the density of dark matter and the number density of galaxies and tidal fragments all peak. Clusters like C09 and C10 are clearly two clusters undergoing mergers, and each one has two separate cores. Interestingly, in the case of C09, one core has a large number of tidal fragments, while the other core has very few. In all cases, we notice that the tidal fragments are much more centrally concentrated than the galaxies. We calculated separately the galaxy and interstellar luminosities for all clusters. The results are shown in Figure 12, for the same subset of clusters as in Figure 11. It is clear that,

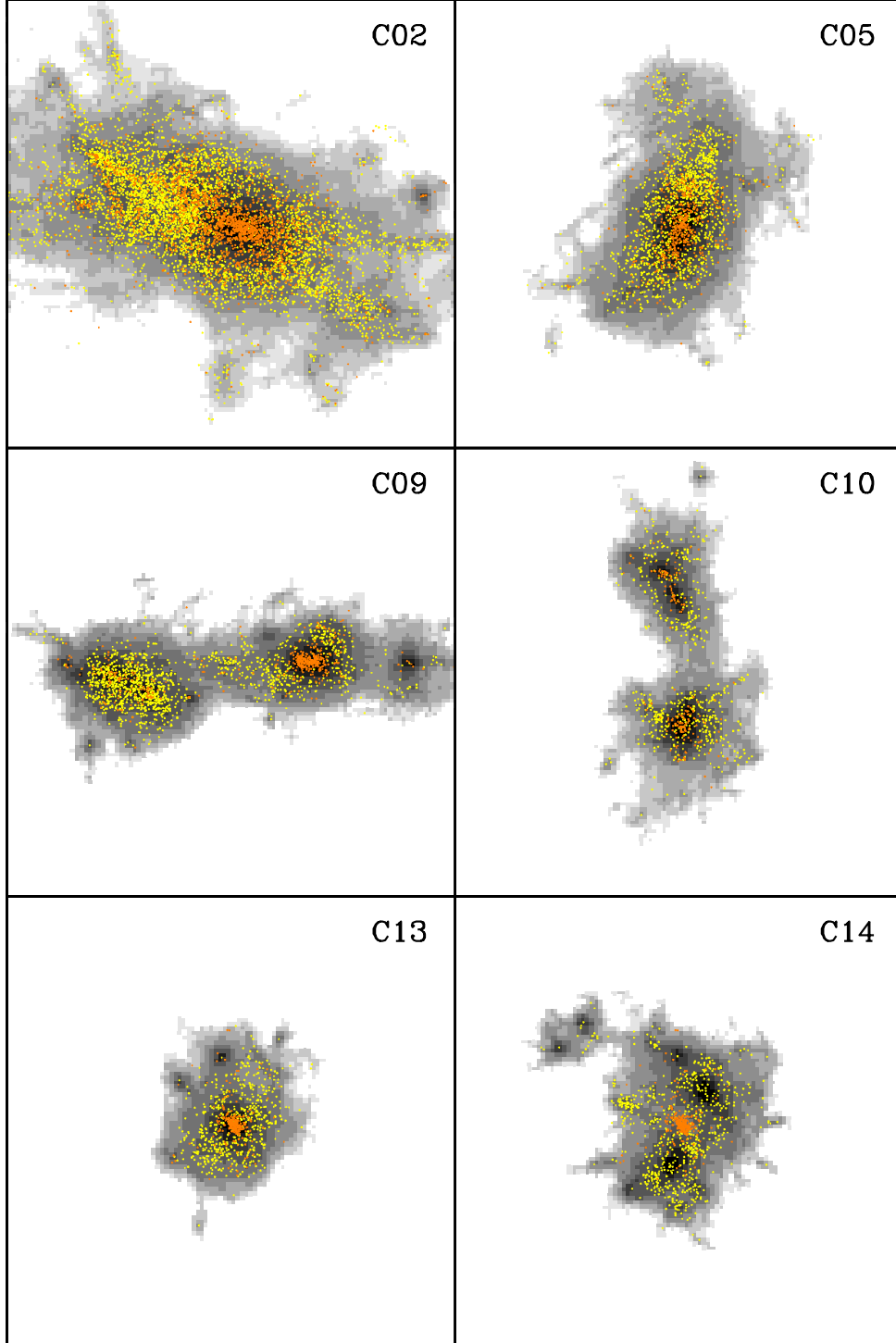


Fig. 11.— Projected maps of some clusters. The greyscale shows the projected surface density of dark matter (shades are separated by 0.3 dex). Yellow and orange dots show galaxies and tidal fragments, respectively. All panels are $8\text{ Mpc} \times 8\text{ Mpc}$.

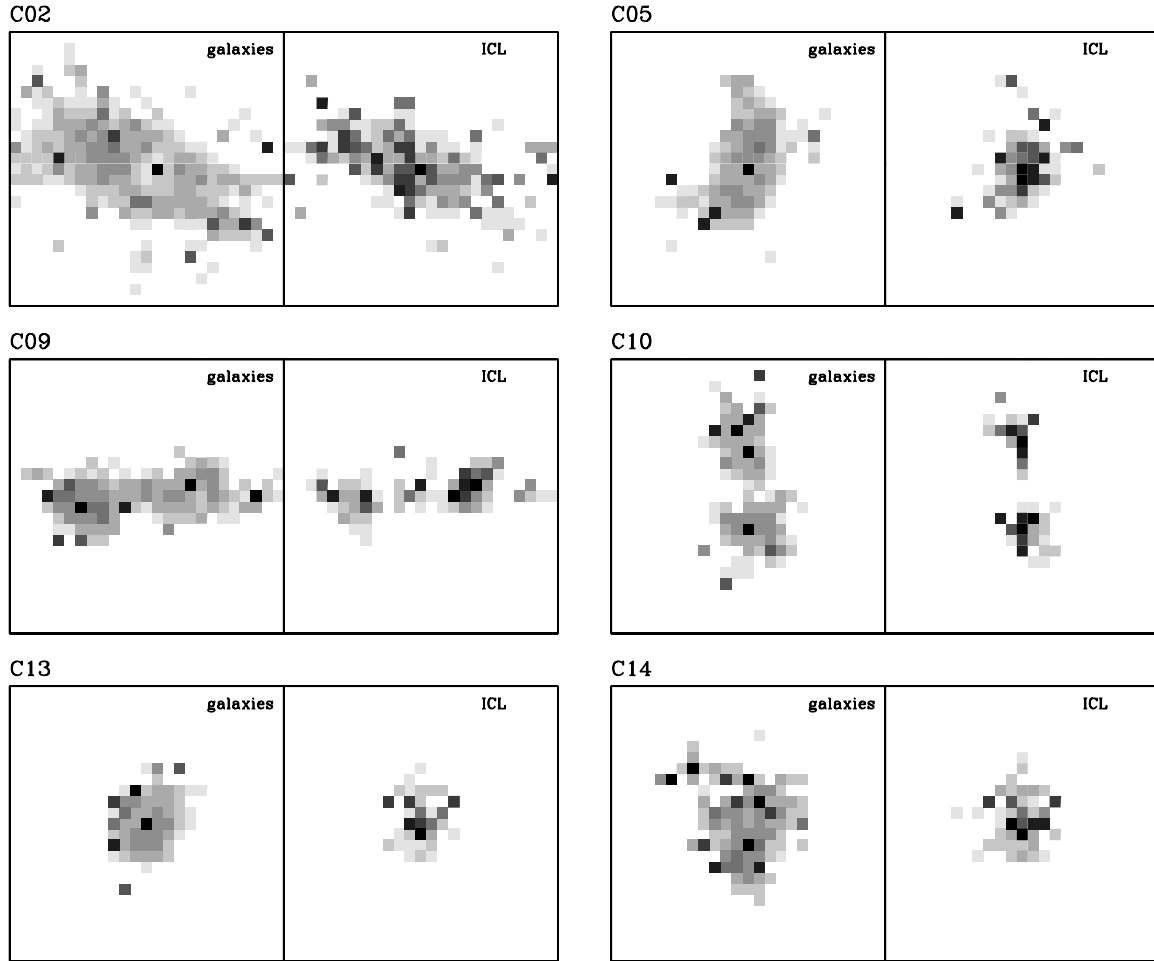


Fig. 12.— Projected luminosity maps of some clusters. The greyscale shows the projected luminosity density of galaxies (left panel for each cluster) and intracluster light (right panel for each cluster). Shades are separated by 0.5 dex, and for each cluster, galaxies luminosity and ICL are plotted using the same greyscale. All panels are 8 Mpc \times 8 Mpc.

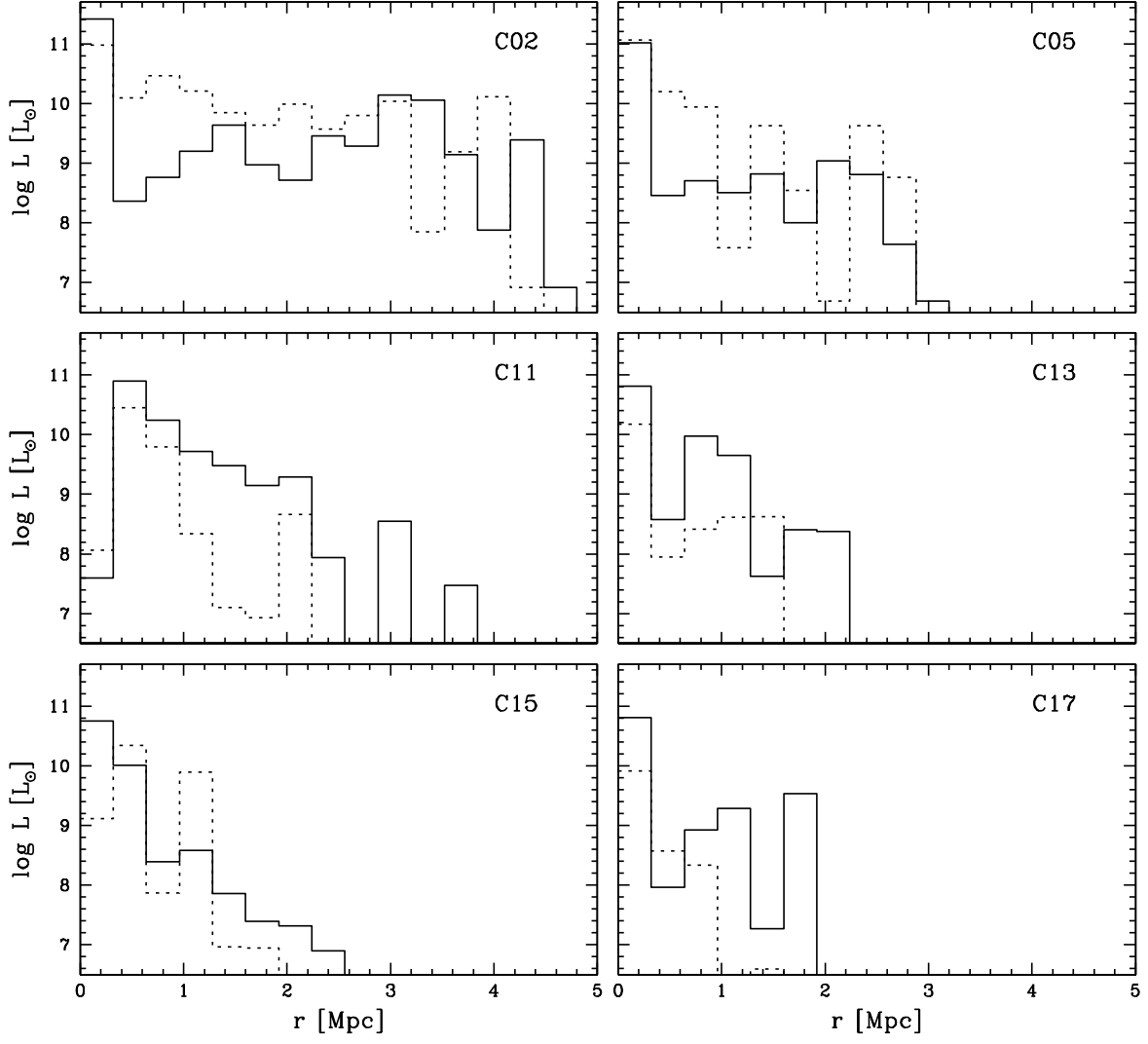


Fig. 13.— Luminosity in projected radial bins for some clusters. Solid and dotted lines show the galactic luminosity and intracluster luminosity, respectively.

within each core, the intracluster light is more concentrated than the galactic light.

We selected all clusters that have a single dominant core. For each cluster, we calculated the position of the projected center-of-light, both for the galactic and ICL components. We then calculated the luminosity of each component in projected radial bins of width 320 kpc. We show some of the results in Figure 13. The central galaxy luminosity tends to be dominated by a bright central galaxy³. Cluster C11 has two bright galaxies located on opposite sides of the center, which explains the low luminosity of the central bin. The profiles show large variations due to the clumpiness of the projected luminosity distributions, but there are some clear trends. For the massive clusters C02 and C05, if we exclude the central bin, the histograms tend to be flat for the galactic luminosity and decreasing for the intracluster luminosity, indicating that the latter is more centrally concentrated. This is even clearer for the lower-mass clusters C11, C13, C15, and C17. Both the galactic luminosity and intracluster luminosity decrease with radius, but the length scale of the intracluster light is of order 0.5 – 0.7 of the length scale of the galactic light. As we saw in Figure 6, the destruction of intermediate-mass galaxies is the primary contributor to the intracluster light. These galaxies can only be destroyed by more massive ones, and these massive galaxies tend to reside in the center of clusters.

Notice that, in our algorithm, tidal fragments are treated as single particles. When a galaxy is tidally destroyed, the algorithm flags it as a tidal fragment with the same mass. Intermediate-mass tidal fragments might be subject to mass segregation, which in this case would be a spurious algorithmic effect, leading to an overestimate of the concentration of ICL in the central region. Still, if most tidal fragments are produced by interactions taking place in the center of clusters, we do expect the fragments to be found in these regions at later time, whether they are represented by one massive particles or several less massive ones.

4. DISCUSSION

Our model combines a gravitational N-body algorithm, a subgrid treatment of galaxy formation, galaxy mergers, and tidal destruction, and a fitting formula for M/L vs. M derived from observations. The greatest virtue of this model is its simplicity. By only including gravitational dynamics, and by using a subgrid treatment at small mass scales, we are able to perform a large cosmological simulation at relatively low computational cost. We simulate a cubic volume of 100 Mpc in size, containing 18 clusters of mass above $10^{14}M_{\odot}$. Doing a full hydrodynamical simulation of this size, without subgrid physics, that could resolve in detail galactic mergers and tidal destruction at the dwarf galaxy scale would be prohibitive. Our simulation only took a few weeks on a 16-processor computer.

There are some caveats implied by the method we use. By only including gravity, and not

³As we explained in § 3.1, that “galaxy” is actually several galaxies represented by one particle.

hydrodynamics, our algorithm can describe the structure and evolution of the mass distribution in the universe, but not how this mass is converted to light. Hence, the algorithm cannot predict the luminosity of galaxies self-consistently. This is why we used the observed relation between M/L and M [eq. (11)] to calculate the luminosity of galaxies and tidal fragments. Actually, this relation gives the *average* value of M/L . For any particular value of M , there is a distribution of values of M/L (Yang et al. 2003). We ignored this, and calculated the luminosity L of an object of mass M by using equation (11) directly. We could instead have used the actual distribution of values of M/L and draw a random value from that distribution for each object, but that would have been an overkill. We formed 1,088,797 dwarf galaxies in our simulation, and by $z = 0$, each massive cluster ($M > 10^{14} M_{\odot}$) contains between 311 and 7,765 galaxies, and between 91 and 2,113 tidal fragments. Drawing the ratios M/L from a distribution instead of using the average value would hardly make any difference in the total luminosity of these components, and the inferred intracluster light fraction f_{ICL} .

Using a subgrid model for galaxy mergers and tidal destruction enables us to reach dwarf-galaxy scales while simulating a large cosmological volume, but there is also another advantage: it provides an unambiguous determination of the outcome of each close encounter (merger, tidal destruction, or simple encounter). If the encounters were actually simulated in details, the determination of their outcome would require detailed analysis, as some of the matter would merge, while some would be ejected, and some of that ejected matter would be reaccreted. As we argue here, and also in Paper I, our subgrid model would not be appropriate to describe a single encounter, but can correctly describe, in a statistical way, the collective effect of a large number of encounters. In the simulation presented in this paper, 590,262 encounters resulted in a merger, 8,314 encounters resulted in tidal destruction followed by dispersion, and 113,132 encounters resulted in tidal destruction followed by accretion.

We have assumed that the intracluster light is caused entirely by galaxies that are tidally destroyed. Some simulations suggest that luminous matter can also be added to the intracluster space during mergers (e.g. Murante et al. 2007). Since we are neglecting this effect, our values of f_{ICL} might be underestimated. However, we could argue that a merger with some of the matter being dispersed in the ICL, a case we do not consider, is an intermediate case between a tidal destruction with complete dispersal of the fragments and a tidal destruction with all the fragments being subsequently reaccreted, two cases we do consider. Hence, two mergers with some of the matter dispersed in the intracluster space could be equivalent to a tidal destruction with complete dispersal of the fragments plus a tidal destruction with complete reaccretion of the the fragments. Statistically, the net effect might be the same.

Our model has only one parameter that is truly tunable: the coefficient Ψ appearing in equation (2). We adjusted this value to reproduce the high-luminosity end of the luminosity function, as seen in Figure 1. Using a larger value of Ψ might lead to an improvement of the luminosity function at the low-luminosity end, but could worsen the fit at the high-luminosity end. Also, a larger value of Ψ would likely result in an increase in both L_{gal} and L_{ICL} , while having a smaller

effect on the value of f_{ICL} .

5. SUMMARY AND CONCLUSION

We performed a numerical simulation of the formation of galaxies and clusters, the destruction of galaxies by mergers and tides, and the evolution of the galactic, extragalactic, and intracluster light, inside a cosmological volume of size $(100 \text{ Mpc})^3$, in a Λ CDM universe. Our main results are the following:

- Our simulation reproduces the observed Schechter luminosity function for luminosities $L > 10^{8.5} L_{\odot}$, up to $L = 10^{11} L_{\odot}$. We have a significant excess of galaxies at luminosities $L < 10^{6.5} L_{\odot}$, and a deficit in the range $10^{6.5} L_{\odot} - 10^{8.5} L_{\odot}$. We attribute this to the discreteness of the galaxy masses. All galaxies in our simulation have masses that are multiples of $M_{\text{min}} = 2 \times 10^9 M_{\odot}$, and this can affect the luminosity function at low L .
- The number of mergers and tidal destruction events increase exponentially with decreasing redshift, with mergers starting at $z \sim 5.9$ and tidal destruction starting at $z \sim 4.8$. This delay is caused by the time it takes to build up galaxies of significantly different masses. Mergers outnumber tidal destruction events by about an order of magnitude, at all redshifts up to the present. When tidal destruction occurs, dispersal of the fragments into the intracluster space dominates over reaccretion of the fragments by the larger galaxy, up to redshift $z \sim 0.5$. This trend is then reversed.
- Tidal destruction is not limited to dwarf galaxies. Intermediate-mass galaxies and even high-mass galaxies are destroyed during encounters with even higher-mass galaxies. Tidal destruction and also mergers involve galaxy pairs with all masses and all mass ratios. We found an interesting trend for encounters between high-mass galaxies ($M > 3 \times 10^{11} M_{\odot}$, $M_{\text{st}} > 5 \times 10^9 M_{\odot}$). The outcome of such encounter seems to depend almost entirely on the mass ratio between the galaxies. Small mass ratios ($m_2/m_1 < 1.2$) result in mergers, intermediate mass ratios ($m_2/m_1 < 10$) result in tidal destruction with the fragment being dispersed into the intracluster space, and higher mass ratios result in tidal destruction, with the fragments being reaccreted by the massive galaxy.
- Most galaxies destroyed by tides are low-mass galaxies. However, the total luminosity provided by these low-mass galaxies is small. 57.9% of the ICL comes from galaxies of intermediate masses ($M = 10^{11} M_{\odot} - 10^{12} M_{\odot}$, $M_{\text{st}} = 6 \times 10^8 M_{\odot} - 2 \times 10^{10} M_{\odot}$), while lower-mass galaxies provide only 11.5% of the ICL. Essentially, the bulk of the ICL comes from galaxies of masses $m_1 = 10^{11} M_{\odot} - 10^{12} M_{\odot}$ which are tidally destroyed by galaxies of mass $m_2 = (1.2 - 10.0)m_1$. Higher mass ratios result in reaccretion of the tidal fragments.
- The present intracluster light fraction f_{ICL} is in the range 1% – 58%. This is consistent with observations, and with simulations presented by other groups. Even though mergers

outnumber tidal destruction events by an order of magnitude, the latter are sufficient to explain the observed ICL. The galaxy luminosity L_{gal} and intracluster luminosity L_{ICL} both increase with cluster mass. The intracluster light fraction f_{ICL} does not show any particular trend with cluster mass, except for the fact that we did not find massive clusters with low values of f_{ICL} .

- The value of f_{ICL} for any particular cluster tends to increase with time. However, some clusters experience sudden drops in f_{ICL} , that can happen at any redshift. At early times, these sudden drops are caused by major mergers, when the cluster absorbs another cluster of comparable mass but with a smaller value of f_{ICL} . At late times, they are caused by a sudden increase in galaxy formation not accompanied by a corresponding increase in tidal destruction.
- Several clusters are not relaxed at $z = 0$, and show complex structures with multiple cores. Focusing on the clusters with a well-defined core, we found that the distribution of ICL is more concentrated than the distribution of galactic light. Most of the ICL comes from intermediate-mass galaxies destroyed by massive ones. Since these massive galaxies tend to reside in the center of clusters, this explains a relatively small extent of the ICL.

This work benefited from stimulating discussions with J. Navarro. All calculations were performed at the Laboratoire d’astrophysique numérique, Université Laval. We thank the Canada Research Chair program and NSERC for support. PB acknowledges support from the FP7 ERC Starting Grant *cosmoIGM*. HM is thankful to the Department of Physics and Astronomy, University of Victoria, for its hospitality.

REFERENCES

- Aguerri, J. A. L., Gerhard, O. E., Arnaboldi, M., Napolitano, N. R., Castro-Rodriguez, N., & Freeman, K. C. 2005, *AJ*, 129, 2585
- Arnaboldi, M., et al. 1996, *ApJ*, 472, 145
- Arnaboldi, M., et al. 2003, *AJ*, 125, 514
- Arnaboldi, M. 2004, *IAU Symposium No. 217*, p. 54
- Arnaboldi, M., Gerhard, O., Aguerri, J. A. L., Freeman, K. C., Napolitano, N. R., Okamura, S., & Yasuda, N. 2004, *ApJ*, 614, L33
- Bahcall, N. A., & Cen, R. 1993, *ApJ*, 407, L49
- Baldry, I. K., Glazebrook, K., & Driver, S. P. 2008, *MNRAS*, 388, 945
- Barai, P., Brito, W., & Martel, H. 2009, *J. Astrophys. Astron.*, 30, 1 (Paper I)
- Behroozi, P. S., Conroy, C., & Wechsler, R. H. 2010, *ApJ*, 717, 379
- Bell, E. F., McIntosh, D. H., Katz, N., & Weinberg, M. D. 2003, *ApJS*, 149, 289
- Bernstein, G. M., Nichol, R. C., Tyson, J. A., Ulmer, M. P., & Wittman, D. 1995, *AJ*, 110, 1507
- Blaauw, A. 1961, *Bull. Astr. Ins. Netherlands*, 15, 265
- Castro-Rodriguez, N., Aguerri, J. A. L., Arnaboldi, M., Gerhard, O., Freeman, K. C., Napolitano, N. R., & Capaccioli, M. 2003, *A&A*, 405, 803
- Conroy, C., Wechsler, R. H., & Kravtsov, A. V. 2007, *ApJ*, 668, 826
- Dolag, K., Murante, G., & Borgani, S. 2010, *MNRAS*, 405, 1544
- Durrell, P. C., Ciardullo, R., Feldmeier, J. J., Jacoby, G. H., & Sigurdsson, S. 2002, *ApJ*, 570, 119
- Feldmeier, J. J., Ciardullo, R., Jacoby, G. H., & Durrell, P. R. 2003, *ApJS*, 145, 65
- Feldmeier, J. J., Ciardullo, R., Jacoby, G. H., & Durrell, P. R. 2004a, *ApJ*, 615, 196
- Feldmeier, J. J., Mihos, J. C., Morrison, H. L., Harding, P., Kaib, N., & Dubinski, J. 2004b, *ApJ*, 609, 617
- Ferguson, H. C., Tanvir, N. R., & von Hippel, T. 1998, *Nature*, 391, 461
- Firmani, C., & Tutukov, A. 1992, *A&A*, 264, 37
- Gal-Yam, A., et al. 2003, *AJ*, 125, 1087

- Gerhard, O. et al. 2005, *ApJ*, 621, L93
- Gnedin, O. 2003, *ApJ*, 582, 141
- Gonzalez, A. H., Zabludoff, A. I., Zaritsky, D. 2005, *ApJ*, 618, 195
- Crane, P., Tammann, G., & Woltjer, L. 1977, *Nature*, 265, 124
- Gregg, M. D., & West, M. J. 1998, *Nature*, 396, 549
- Gvaramadze, V. V., Gualandris, A., & Portegies Zwart, S. 2010, *IAU Symposium*, Volume 266, p. 413-416
- Hatch, N. A., Overzier, R. A., Röttgering, H. J. A., Kurk, J. D., & Miley, G. K. 2008, *MNRAS*, 383, 931
- Henriques, B. M., Bertone, S., & Thomas, P. A. 2008, *MNRAS*, 383, 1649
- Krick, J. E., Bernstein, R. A., & Pimbblet, K. A. 2006, *AJ*, 131, 168
- Krick, J. E., & Bernstein, R. A. 2007, *AJ*, 134, 466
- Lin, Y.-T., & Mohr, J. J. 2004, *ApJ*, 617, 879
- Mihos, J. C., Harding, P., Feldmeier, N., & Morrison, H. 2005, *ApJ*, 632, L41
- Murante, G., et al. 2004, *ApJ*, 607, L83
- Murante, G., Govioli, M., Gerhard, O., Arnaboldi, M., Borgani, S., & Dolag, K. 2007, *MNRAS*, 377, 2
- Napolitano, N. R. et al. 2003, *ApJ*, 594, 172
- Neill, J. D., Shara, M. M., & Oegerle, W. R. 2005, *ApJ*, 618, 692
- Poveda, A., Ruiz, J., & Allen, C. 1967, *Bol.Obs.Tonantzintla Tacubaya*, 4, 86
- Puchwein, E., Springel, V., Sijacki, D., & Dolag, K. 2010, *MNRAS*, 406, 936
- Purcell, C. W., Bullock, J. S., & Zentner, A. R. 2007, *ApJ*, 666, 20
- Rudick, C. S., Mihos, J. C., Frey, L. H., McBride C. K. 2009, *ApJ*, 699, 1518
- Rudick, C. S., Mihos, J. C., & McBride, C. K. 2006, *ApJ*, 648, 936
- Rudick, C. S., Mihos, J. C., & McBride, C. K. 2011, *ApJ*, 732, 48
- Scheick, X., & Kuhn, J. R. 1994, *ApJ*, 423, 566
- Sommer-Larsen, J., Romeo, A. D., & Portinari, L. 2005, *MNRAS*, 357, 478

- Springel, V. et al. 2005, *Nature*, 435, 629
- Stadel, J. G. 2001, PhD Thesis (University of Victoria)
- Sun, M., Donahue, M., Roediger, E., Nulsen, P. E. J., Voit, G. M., Sarazin, C., Forman, W., & Jones, C. 2010, *ApJ*, 708, 946
- Thuan, T. X., & Kormendy, J., 1977, *PASP*, 89, 466
- Tinker, J., Kravtsov, A. V., Klypin, A., Abazajian, K., Warren, M., Yepes, G., Gottlöber, S., & Holz, D. E. 2008, *ApJ*, 688, 709
- Tutukov, A. V., & Fedorova, A. V. 2009, *Astronomy Reports*, 53, 839
- Tutukov, A. V., & Fedorova, A. V. 2011, *Astronomy Reports*, 55, 383
- Tyson, J. A., & Fischer, P. 1995, *ApJ*, 446, L55
- Uson, J. 1991, *ApJ*, 369, 46
- Vilchez-Gomez, R. 1994, *A&A*, 283, 37
- Weil, M. L., et al. 1997, *ApJ*, 490, 664
- West, M. J., Côté, P., Jones, C., Forman, W., & Marzke, R. O. 1995, *ApJ*, 453, L77
- Williams, B. F. et al. 2007, *ApJ*, 656, 756
- Willman, B., Governato, F., Wadsley, J., & Quinn, T. 2004, *MNRAS*, 355, 159
- Wu, Y.-T., & Jiang, I.-G. 2009, *MNRAS*, 399, 628
- Yang, X., Mo, H. J., & van den Bosch, F. C. 2003, *MNRAS*, 339, 1057
- Yang, X., Mo, H. J., & van den Bosch, F. C. 2009, *MNRAS*, 693, 830
- Zibetti, S., White, S. D. M., Schneider, D. P., & Brinkmann, J. 2005, *MNRAS*, 358, 949
- Zwicky, F. 1951, *PASP*, 63, 61